

ULTRAFast TUNABLE MICROWAVE FILTER  
PHASE II, TASK 2

552,848

(5)

Adolph Presser  
RCA Laboratories  
David Sarnoff Research Center  
Princeton, New Jersey 08540

APRIL 1982

Final Report for Period 15 May 1980 to 30 April 1982

Prepared for  
Department of the Navy  
Naval Research Laboratory  
Washington, D.C. 20375

DTIC FILE COPY

APPROVED FOR PUBLIC RELEASE  
DISTRIBUTION UNLIMITED

91 4 09 001

REPORT DOCUMENTATION PAGE		READ INSTRUCTIONS BEFORE COMPLETING FORM
1. REPORT NUMBER	2. GOVT ACCESSION NO.	3. RECIPIENT'S CATALOG NUMBER
4. TITLE (and Subtitle)  ULTRAFast TUNABLE MICROWAVE FILTER		5. TYPE OF REPORT & PERIOD COVERED Final Report (5-15-80 to 4-30-82)
		6. PERFORMING ORG. REPORT NUMBER RCA-PRRL-81-CR-33
7. AUTHOR(s)  A. Presser		8. CONTRACT OR GRANT NUMBER(s)  N00173-79-C-0186
9. PERFORMING ORGANIZATION NAME AND ADDRESS RCA Laboratories Princeton, New Jersey 08540		10. PROGRAM ELEMENT, PROJECT, TASK AREA & WORK UNIT NUMBERS  Phase II, Task 2
11. CONTROLLING OFFICE NAME AND ADDRESS Department of the Navy Naval Research Laboratory Washington, DC 20375		12. REPORT DATE November 1981
		13. NUMBER OF PAGES 73
14. MONITORING AGENCY NAME & ADDRESS (if different from Controlling Office)		15. SECURITY CLASS. (of this report) Unclassified
		15a. DECLASSIFICATION/DOWNGRADING SCHEDULE N/A
16. DISTRIBUTION STATEMENT (of this Report)  <b>APPROVED FOR PUBLIC RELEASE DISTRIBUTION UNLIMITED</b>		
17. DISTRIBUTION STATEMENT (of the abstract entered in Block 20, if different from Report)		
18. SUPPLEMENTARY NOTES		
19. KEY WORDS (Continue on reverse side if necessary and identify by block number) Filter Voltage tunable Varactor FET two-section filter		
20. ABSTRACT (Continue on reverse side if necessary and identify by block number) * Varactor-tunable resonant filter elements that use the negative resistance of an FET to overcome the losses of the varactor and the circuit were used to construct two two-section filters. The two filters operate in the 8.2- to 10.3-GHz frequency range. The tuning bandwidth of both filters is 2.0 GHz. Typically, the midband insertion loss over the tuning band is 0 ±2 dB; the 3-dB bandwidth is 29 ±11 MHz.		

## PREFACE

This final report describes the work done at the Microwave Technology Center of RCA Laboratories during the period from 15 May 1980 to 30 April 1982, in performance of a Phase II, Task 2 program, sponsored by the Naval Electronics System Command, directed by the Naval Research Laboratory under Contract No. N00173-79-C-0186. The work of Phase II, Task 1, covering the period from 1 June 1979 to 15 May 1980, was described earlier in a separate interim report. F. Sterzer is the Center's Director, E. F. Belohoubek was the Project Supervisor, and A. Presser was the Project Scientist.

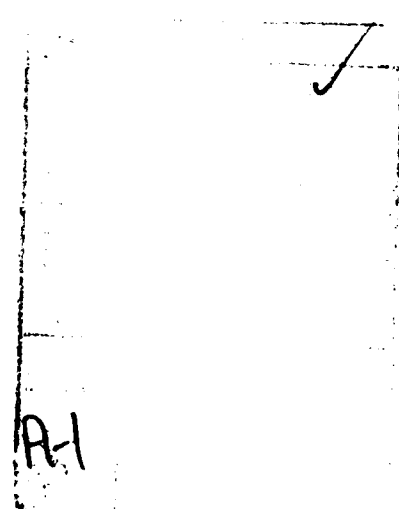


# TABLE OF CONTENTS

Section	Page
I. INTRODUCTION .....	1
II. FILTER DESIGN .....	3
A. Design Approach .....	3
B. Filter Components .....	5
1. Resonant Element .....	5
a. Varactor .....	5
b. Negative-Resistance FET Circuit .....	5
c. Construction .....	8
2. Coupling Networks .....	9
a. Unsymmetric Divider .....	9
b. Symmetric Impedance Inverter .....	10
C. History of Resonant-Element Development .....	11
D. Experimental Element Evaluation .....	15
1. Selectivity .....	19
2. Tuning Range .....	21
3. Signal Input Effects .....	23
4. Noise Figure .....	25
5. Temperature Effects .....	27
6. Tuning Speed .....	27
E. Prototype Filters .....	29
1. Single-Section Filter .....	30
2. Two-Section Filter .....	30
III. FINAL FILTER PERFORMANCE .....	45
A. Single Element .....	45
B. Two-Section Filter .....	47
IV. CONCLUSIONS AND RECOMMENDATIONS .....	63
REFERENCES .....	64

# LIST OF ILLUSTRATIONS

Figure	Page
1. Block diagram of multisection bandpass filter with impedance inverters .....	4
2. Idealized equivalent circuits of active resonant element .....	4
3. Measured junction capacitance, resistance, and $Q_0$ of typical varactor .....	6
4. Equivalent of negative resistance producing FET circuit .....	6
5. FET equivalent circuit for resonant element simulations .....	7
6. Calculated impedance of FET circuit as shown in Fig. 4 .....	7
7. Resonant element construction: (a) realizable configuration; (b) equivalent circuit of configuration .....	8
8. Unsymmetric impedance divider .....	10
9. Symmetric impedance inverter .....	11
10. Earlier symmetric resonant element realization with two FETs and two varactors .....	12
11. Equivalent circuit of symmetric element .....	13
12. Symmetric element diagram of experimental single-section filter configuration (drain back to back): (a) tuning in drain circuit; (b) tuning in gate circuit .....	14
13. Symmetric element diagram of experimental single-section filter configuration (gate back to back): (a) tuning in gate circuit; (b) tuning in drain circuit .....	14
14. Photographic close-up of final element circuit with one FET and one varactor .....	16
15. Resonant element module .....	17
16. Test fixture for resonant element evaluation .....	18
17. Manual network analyzer test setup for transmission and reflection evaluation .....	20
18. Measured 3-dB bandwidth and VSWR vs midband frequency of single-section filter with high selectivity and small bandwidth deviation over tuning band .....	20
19. Varactor and gate voltages vs midband frequency in broadband tuning experiment with two varactors in series .....	22

# LIST OF ILLUSTRATIONS (Continued)

Figure	Page
20. Measured 3-dB bandwidth and transmission gain vs midband frequency (broadband experiment) .....	22
21. Measured VSWR and transmission gain (broadband experiment) .....	23
22. Measured transmission passband response at a given filter setting for three different input power levels .....	24
23. Test setup to evaluate IMD and other two-signal effects .....	25
24. Measured two-signal intermodulation distortion (absolute and relative) as a function of input power level .....	25
25. Measured noise figure at different frequency settings .....	26
26. Noise figure test setup .....	27
27. Measured effects of temperature upon 3-dB bandwidth, midband frequency, and transmission gain .....	28
28. Test setup to evaluate filter tuning speed .....	29
29. Single-section filter prototype.....	31
30. Varactor and gate voltage settings vs midband frequency .....	32
31. Measured 3-dB bandwidth vs midband frequency .....	32
32. Measured input and output VSWR vs midband frequency .....	33
33. Measured transmission passband response of single-section filter ( $V_v = 0$ V) .....	33
34. Measured transmission passband response of single-section filter ( $V_v = 5$ V) .....	34
35. Measured transmission passband response of single-section filter ( $V_v = 10$ V) .....	34
36. Measured transmission passband response of single-section filter ( $V_v = 20$ V) .....	35
37. Measured transmission passband response of single-section filter ( $V_v = 30$ V) .....	35
38. Measured transmission passband response of single-section filter (forward and reverse power flow) .....	36
39. Measured input and output reflection coefficient in passband of single-section filter .....	36

# LIST OF ILLUSTRATIONS (Continued)

Figure	Page
40. Measured transmission response of a single-section filter adjusted for high selectivity .....	37
41. Measured phase response in passband of high-selectivity filter .....	37
42. Measured group-delay passband response of high-selectivity filter .....	38
43. Measured VSWR in passband of high-selectivity filter .....	38
44. Two-section filter prototype .....	39
45. Varactor and gate voltage vs midband frequency of each element in two-section prototype filter .....	40
46. Measured 3-dB bandwidth and VSWR vs midband frequency of two-section prototype filter.....	41
47. Measured input and output reflection coefficient passband response of two-section prototype filter .....	41
48. Measured transmission passband response for forward and reverse power flow of two-section prototype filter .....	42
49. Measured passband response of experimental filter with Chebyshev response .....	42
50. Measured selectivity of experimental two-section filter with Chebyshev response .....	43
51. Measured phase passband response of Chebyshev filter .....	43
52. Measured group-delay passband response of Chebyshev filter .....	44
53. Measured passband return loss of Chebyshev filter .....	44
54. Measured midband frequency vs varactor voltage for four different resonant elements .....	45
55. Measured gate voltage for 0-dB transmission loss of four different resonant elements at given varactor voltages .....	46
56. Measured 3-dB bandwidth of four different elements for given varactor voltage settings .....	46
57. Photographic close-up of final two-section filter circuit .....	48
58. Photographic view of final two-section filter .....	49

# LIST OF ILLUSTRATIONS (Continued)

Figure	Page
59. Measured varactor voltages vs midband frequency (final filter No. 1) .....	51
60. Measured gate voltages at midband frequency settings (final filter No. 1) .....	52
61. Measured 3-dB bandwidth and noise figure at midband frequency settings (final filter No. 1) .....	52
62. Measured transmission gain and VSWR at midband frequency settings (final filter No. 1) .....	53
63. Measured transmission passband response for forward and reverse power flow (final filter No. 1) .....	53
64. Measured phase passband response for forward and reverse power flow (final filter No. 1) .....	54
65. Measured input and output reflection coefficient in passband (final filter No. 1) .....	54
66. Measured forward and reverse group delay in passband (final filter No. 1) .....	55
67. Measured midband response for three input power levels (final filter No. 1) .....	55
68. Measured group-delay midband response for three input power levels (final filter No. 1) .....	56
69. Measured varactor voltage for each element at given midband frequencies (final filter No. 2) .....	57
70. Measured gate voltages for each element at given midband frequencies (final filter No. 2) .....	57
71. Measured transmission gain and VSWR vs midband frequency (final filter No. 2) .....	58
72. Measured 3-dB bandwidth and noise figure vs midband frequency (final filter No. 2) .....	58
73. Measured transmission passband response for forward and reverse power flow (final filter No. 2) .....	59
74. Measured phase passband response, forward and reverse (final filter No. 2) .....	59

## LIST OF ILLUSTRATIONS (Continued)

Figure	Page
75. Measured input and output reflection coefficient frequency response (final filter No. 2) .....	60
76. Measured forward and reverse group-delay passband response (final filter No. 2) .....	60
77. Measured midband response for three input power levels (final filter No. 2) .....	61
78. Measured group-delay midband response for three input power levels (final filter No. 2) .....	61

## LIST OF TABLES

Table	Page
1. Two-Section Filter No. 1 .....	51
2. Two-Section Filter No. 2 .....	56

## SECTION I

### INTRODUCTION

Fast, electronically tunable high-Q filters are desirable components for many EW applications. Tuning speed can be gained in these applications with varactor tunable filters in place of the commonly used YIG filters, which are inherently slow. At increasing frequencies above 1 GHz, however, varactor losses in filters limit selectivity severely. The proposed approach to overcome varactor losses with the negative resistance of GaAs FETs was shown to be feasible during the Phase I effort under Contract No. N00173-77-C-0201. These earlier efforts resulted in a single-section filter performance with a 3-dB selectivity of 20 MHz at 9 GHz over a 500-MHz tuning band; two-section operation with this approach was also demonstrated. The subsequent Phase II, Task 1 effort of this program (Contract No. N00173-79-C-0186) used the approaches of Phase I in the successful design and construction of three-section filters tunable over the 9.0- to 9.6-GHz frequency range. The results of this work were reported in a separate interim report covering the period from 1 June 1979 to 15 May 1980.

The goals of the Phase II, Task 2 effort, reported here, were to extend tuning bandwidth capabilities over a multigigahertz frequency band and to demonstrate high-selectivity performance in single-section filters and to design, construct, and deliver two two-section prototype filters with the following performance objectives:

Frequency	7-11 GHz
Filter Pass Bandwidth	30 MHz at 30-dB point
Passband Insertion Loss	$\leq 2$ dB
Tuning Voltage	0-30 V
Tuning Speed	$< 30$ ns

The major contributions of this program were:

- The redesign of the active resonant element to eliminate an inherent coupling mechanism that is detrimental to multisection filter performance.
- The demonstration of a basic 3.6-GHz tuning capability for a single resonant element.

- The successful design and construction of two two-section filters tunable over a 2.0-GHz  $\pm 20$ -MHz frequency band.
- The attainment of 29  $\pm 11$ -MHz selectivity at the 3-dB points.
- The identification of problem areas, like noise figure and saturation effects, to be solved during subsequent efforts.

Two prototype two-section filters were delivered at the end of this program which had the following performance:

	<u>Unit 1</u>	<u>Unit 2</u>
Midband Frequency, $f_o$	8.26-10.25 GHz	8.27-10.30 GHz
3-dB Bandwidth, BW	27 $\pm 9$ MHz	36 $\pm 4$ MHz
Midband Insertion Loss, L	0 $\pm 1$ dB	0 $\pm 2$ dB
Rejection, $f_o \pm 2$ BW	.....24 dB.....	.....
Noise Figure, F	21 $\pm 2$ dB	24 $\pm 1$ dB
Tuning Voltage	.....0-30 V.....	.....
Size	.....38 mm x 35 mm x 20 mm.....	.....

## SECTION II

### FILTER DESIGN

#### A. DESIGN APPROACH

Electronically tunable filters require high-Q elements with tunable reactances. Presently, the magnetically tuned YIG element is most commonly used in the applications at microwave frequencies. The high-Q of YIG resonators assures high selectivity, but the magnetic tuning circuitry limits their tuning speed to the millisecond range. Varactors, which are frequently used at UHF frequencies, can be tuned at rates that are about three orders of magnitude higher than those of the YIG, but their relative losses severely limit selectivity in passive circuits at microwave frequencies.

The approach taken in this program was to overcome the inherent varactor losses with the negative resistance of an active element. The negative resistance of a GaAs FET was originally chosen because of broadband capabilities. The design and results obtained during the Phase I effort [1] substantiated feasibility of this approach generally; the Phase II, Task 1 efforts [2] demonstrated three-section-filter capabilities.

The negative resistance of the FET, the varactor, the necessary tuning inductance, and dc connections are combined on a suitable carrier into a resonant element. These elements are then employed in single- or multisection bandpass filters designed according to standard passive coupled-resonator filter theory [3-5]. The diagram in Fig. 1 depicts a multisection bandpass filter in its basic form. The  $N$  resonant elements  $E$  are connected to the terminating impedances  $R_0$  as shown, via  $(N + 1)$  coupling networks  $K$ . The coupling networks are designed to have impedance transforming properties to

1. A. Presser, "Ultra-Fast Tunable Microwave Filter," Final Report, Contract No. N00173-77-C-0201, Aug. 1978.
2. A. Presser, "Ultra-Fast Tunable Microwave Filter," Final Report, Phase II, Task 1, Contract No. N00173-79-C-0186, Aug. 1980.
3. G. L. Matthaei et al., Microwave Filters, Impedance-Matching Networks and Coupling Structures (McGraw-Hill Book Co., 1964), p. 421.
4. J. F. Cline et al., "Tunable Passive Multi-Couplers Employing Minimum Loss Filters," IRE Trans. PGMTT-7, 121 (Jan. 1959).
5. S. B. Cohn, "Dissipation Loss in Multiple-Coupled Resonator Filter," Proc. IRE 47, 1342 (Aug. 1959).

give the required N-section filter response. The resonant element E in its ideal form can be represented by the circuit diagram shown in Fig. 2. The varactor and its losses are represented by the capacitor  $C_V$  and the resistor  $R_V$ , respectively. The FET with its feedback configuration is represented by the impedance Z, which has a negative real part. The inductor  $L_T$  finally brings the combination of all parameters into resonance. The following paragraphs of this section describe the design, construction, and performance of the major filter components, as well as element construction and performance.

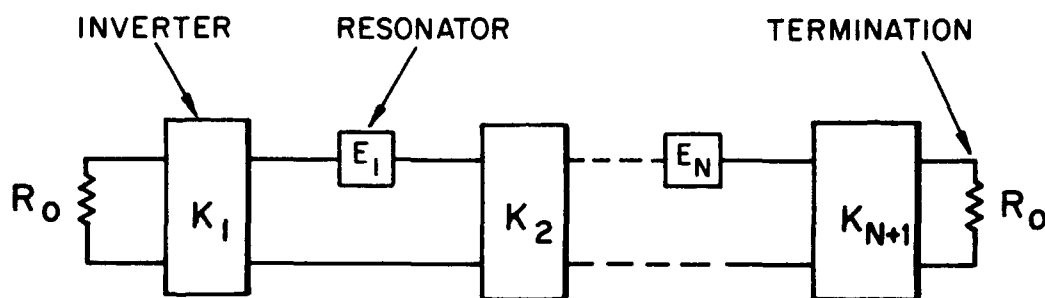


Figure 1. Block diagram of multisection bandpass filter with impedance inverters.

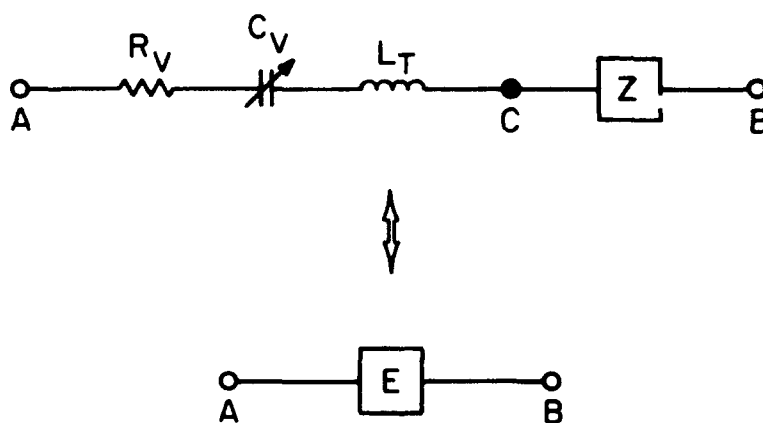


Figure 2. Idealized equivalent circuits of active resonant element.

## B. FILTER COMPONENTS

A filter as depicted in Fig. 1 consists of two major components, the resonant elements E and the coupling networks K. These major components and their subcomponents are described in this paragraph.

### 1. Resonant Element

#### a. Varactor

Generally, the most important varactor parameters are junction capacitance ( $C_j$ ) variation with bias voltage, breakdown voltage, and series resistance. These parameters are rather predictable and depend upon varactor construction [6]. The particular varactor chosen for this program was an inexpensive abrupt-junction Si-varactor in chip form (Part #GC-1500A-00)\* with a capacitance ratio that is larger than 6:1 between 0 and 30 V ( $C_{j(0)} = 1.42$  pF,  $C_{j(30)} = 0.22$  pF). The plot in Fig. 3 shows the measured junction capacitance and series resistance of this varactor. The series resistance was derived from Q measurements at 1 GHz. Since diode Q varies inversely with frequency, the need to overcome all or most of the varactor losses (1.5 to 2.5  $\Omega$ ) at frequencies near 10 GHz for high-selectivity applications is evident.

#### b. Negative-Resistance FET Circuit

The objective to attain an impedance element with a negative real part of 1.5 to 2.5  $\Omega$  was met with an FET in an arrangement shown in Fig. 4. The circuit element values were chosen to operate the FET in a common drain configuration that provides negative resistance over the largest range of frequencies.

When an FET model [7] was used (see Fig. 5), calculations for the impedance between terminals B and C of Fig. 4 without the capacitor  $C_F$  show that this FET circuit can be represented by a parallel circuit of a relatively large negative resistance (50 to 200  $\Omega$ ) and a small capacitance ( $\sim 0.07$  pF).

6. P. Penfield, Jr., and R. P. Rafuse, Varactor Applications (MIT Press, Cambridge, MA, 1962).

7. P. Wolf, "Microwave Properties of Schottky-Barrier Field-Effect Transistors," IBM J. Res. Dev. 14, 125 (March 1970).

\*GHZ Devices, Inc., S. Chelmsford, MA.

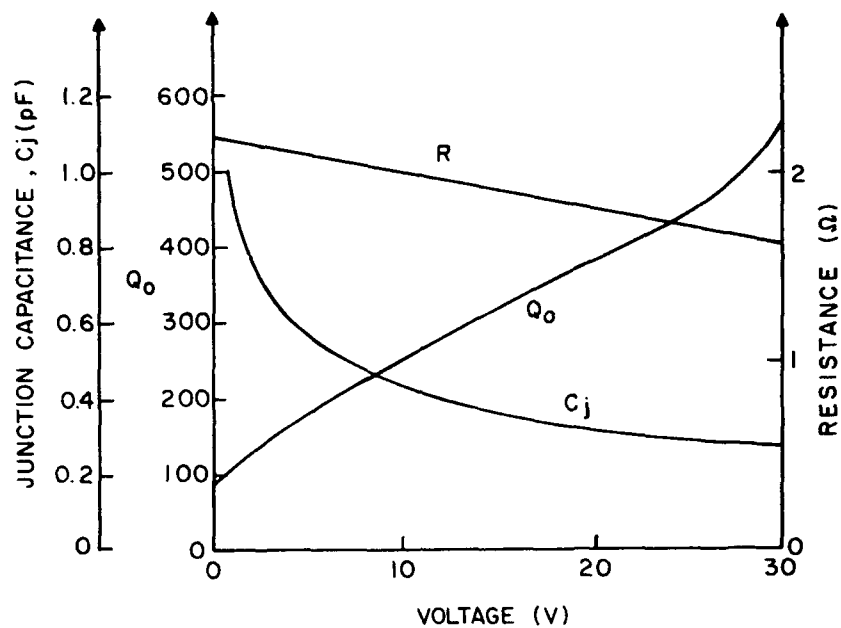


Figure 3. Measured junction capacitance, resistance, and  $Q_o$  of typical varactor.

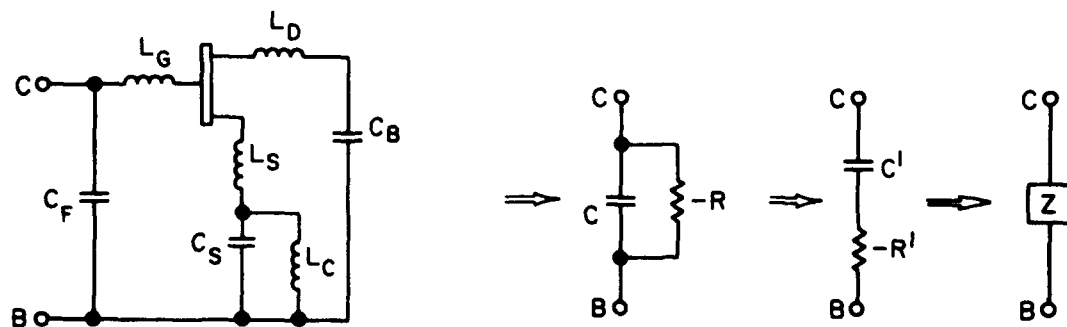


Figure 4. Equivalent of negative resistance producing FET circuit.

The capacitor  $C_F$ , therefore, serves two purposes: it Q-transforms the negative resistance to a series value in the desired range, and also prevents effective capacitance ratio reduction of the varactor, which eventually has to be placed in series with the FET circuitry as shown in the element diagram of

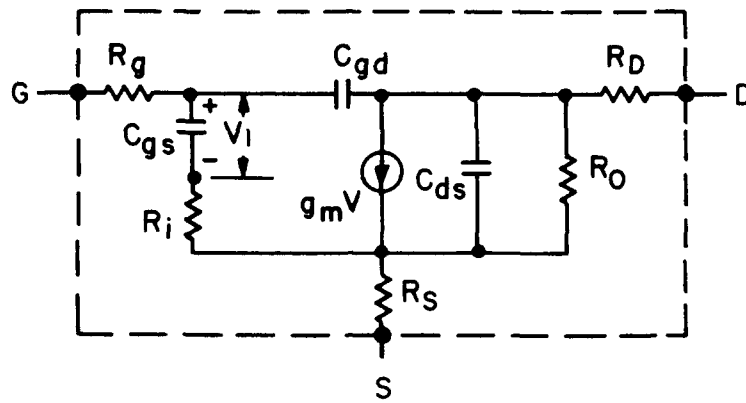


Figure 5. FET equivalent circuit for resonant element simulations.

Fig. 2. The results of a sample calculation for the complete circuit of Fig. 4 in the 7- to 12-GHz frequency range is shown in Fig. 6 for two values of  $C_F$  (0.4 and 0.6 pF).

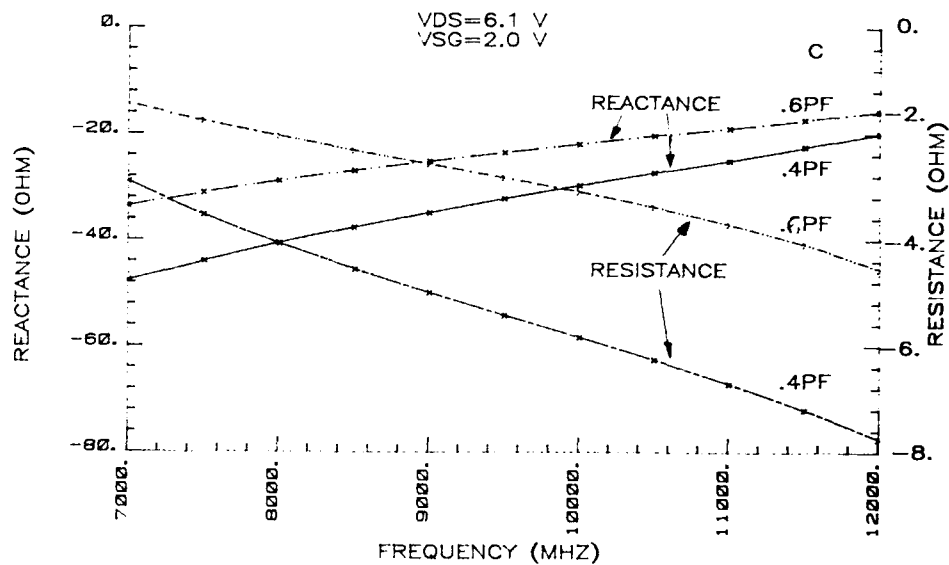


Figure 6. Calculated impedance of FET circuit as shown in Fig. 4.

### c. Construction

The varactor and the negative-resistance circuitry are combined on a common carrier to obtain a series-resonant high-Q element that serves as a building block for multisection bandpass filter designs. The carrier must have small parasitic effects upon resonance and permit easy access to the required external bias and tuning voltages. Figure 7(a) shows a realizable assembly of the resonant element that fulfills the essential carrier requirements. The varactor, the negative-resistance circuitry, and the tuning inductance are fabricated on an alumina wafer. Metallic thin-film circuits support the varactor, the FET, and all associated circuit components as shown on the sketch (Fig. 7). Wire bonds representing lumped-element inductors are used to interconnect the individual components. Also shown on the sketch [Fig. 7(b)] is an electrically equivalent circuit of this element.

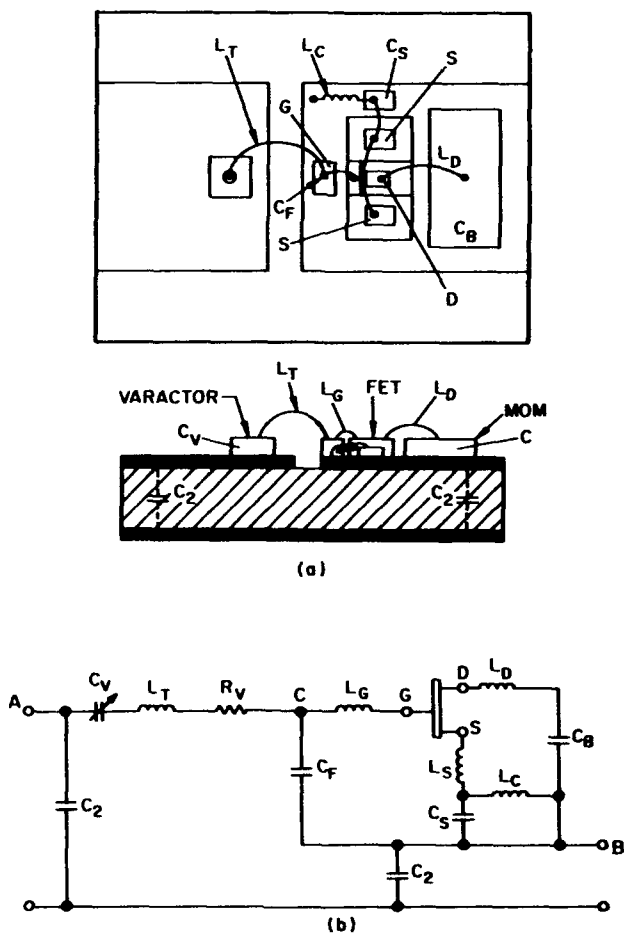


Figure 7. Resonant element construction: (a) realizable configuration; (b) equivalent circuit of configuration.

This realization differs electrically from the ideal-element representation in Fig. 2 by the carrier pad capacitances  $C_2$  to ground of the metallized alumina wafer; this produces a four-terminal structure. The capacitances  $C_2$  are, as will be shown later, absorbed into the coupling networks of the filter. In the final realization of the element, thin-film technology is used to print the necessary dc connections for the FET and varactor onto the carrier.

## 2. Coupling Networks

The coupled-resonator design approach requires the use of impedance inverters. These inverters transform the terminating loads to the resonator, and/or couple individual resonators as needed to attain the desired response shape for multisection bandpass filters. In the following paragraphs, some realizable impedance inverter circuits, found useful in element testing and construction of the final two-section filters, are described.

The basic requirements for an ideal impedance inverter are a real image impedance in the frequency range of operation and an image phase that is an odd multiple of  $\pm 90^\circ$ . One of the simplest inverter circuits, for instance, is a quarter-wavelength transmission line. It has an inverter parameter  $K$  of  $Z_0 \Omega$  (the characteristic impedance of the line) and an overall phase shift of  $90^\circ$  at some frequency  $f_0$  and its odd multiples. The use of such lines was precluded in the final design because of size and bandwidth limitations. Two other types of inverters, an unsymmetric divider type and a symmetric type, were used in this program.

### a. Unsymmetric Divider

The general form of this divider is shown in Fig. 8. Very large down transformation of the terminating resistor  $R$  can be obtained over large frequency ranges if the reactance sum of  $X_1$  and  $X_2$  is large when compared to  $R$ . The relationships between the given and equivalent parameters are also shown in the figure. The specific unsymmetric type that was used is of the capacitive variety in which  $X_1$  is the reactance of a small coupling capacitor  $C_1$ , and  $X_2$ , the reactance of the element carrier-pad capacitance  $C_2$ . The transformed series impedance  $R'$  loading the resonator is

$$R' = \frac{R}{\left(1 + \frac{C_2}{C_1}\right)^2}$$

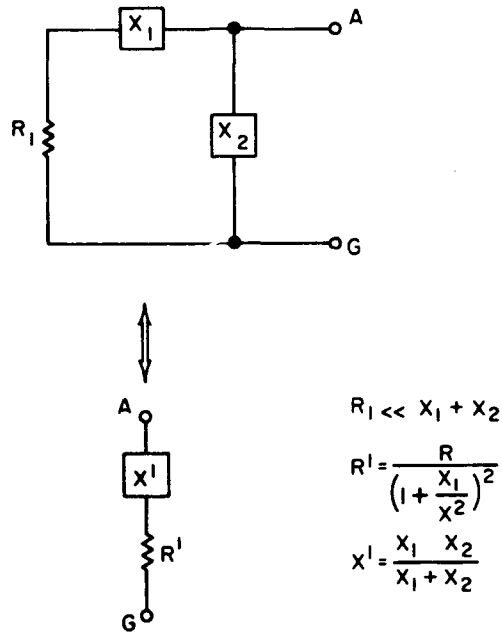


Figure 8. Unsymmetric impedance divider.

and the excess series capacitance to be absorbed by the resonator is  $C' = C_1 + C_2$ . For specific values of  $R = 50 \Omega$ ,  $C_1 = 0.02 \text{ pF}$  and  $C_2 = 0.4 \text{ pF}$ ; the transformed parameters are  $R' = 0.125 \Omega$  and  $C' = 0.42 \text{ pF}$ .

#### b. Symmetric Impedance Inverter

The general form of a symmetric impedance inverter is shown in Fig. 9(a). The shunt element  $Z$  is practically realizable in inductive or capacitive form. The parameter values  $Z'$  are computable from a bisection of the network by use of the basic inverter requirements with open- and shorted-circuit conditions. These parameters  $Z'$  must be absorbable by the resonators and/or the loads. In the lossless case, in which the inverter element  $Z$  is purely reactive, the elements  $Z'$  are also reactive and the inverter parameter  $K$  is real. If the element  $Z$  is lossy, the  $Z'$  elements are also lossy and the inverter parameter  $K$  is complex. The general values of  $Z'$  and  $K$  are also given in Fig. 9. The specific realizable inverters in capacitive and inductive form are shown in Figs. 9(b) and 9(c), respectively.

Experimentation with a variety of inverters of this type showed that at X-band frequencies, 100:1 transformations are practical with capacitive elements.

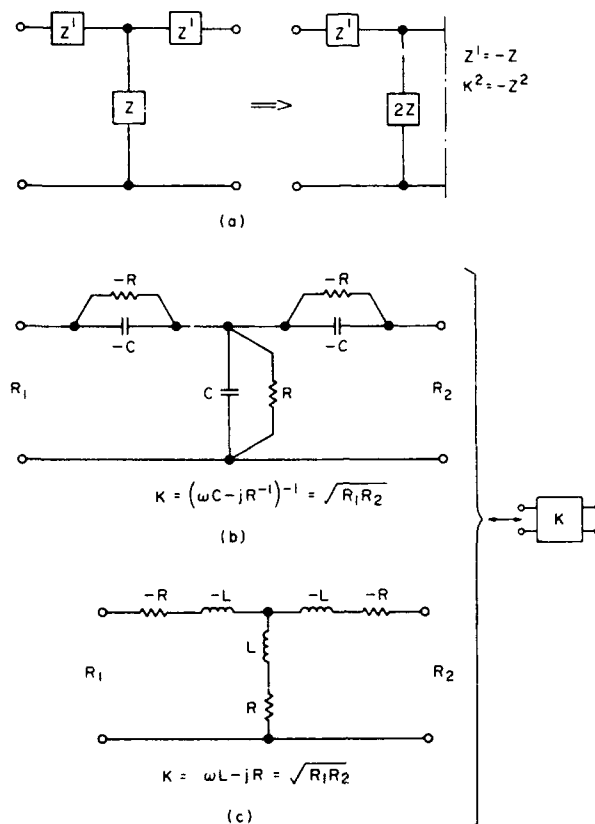


Figure 9. Symmetric impedance inverter.

Similar transformation ratios are feasible with inductive elements, even though the experiments were conducted at a 10:1 ratio only. The importance of the complex K-inverter was discovered in the analysis of an electrically symmetric, negative-resistance resonant element in which excessive detuning and loading effects of the inverter caused unsymmetric frequency responses and limited selectivity.

### C. HISTORY OF RESONANT-ELEMENT DEVELOPMENT

During the earlier part of this program, we used a planar resonant element in an electrically symmetric configuration with two varactors and two FETs. Such an element is shown in Fig. 10, and its equivalent circuit in Fig. 11. Printed rectangular rf-chokes in the dc-connecting circuits with considerable parasitic reactances to ground were responsible for instabilities occasionally observed at frequencies in the 2- to 4-GHz frequency range. To increase tuning

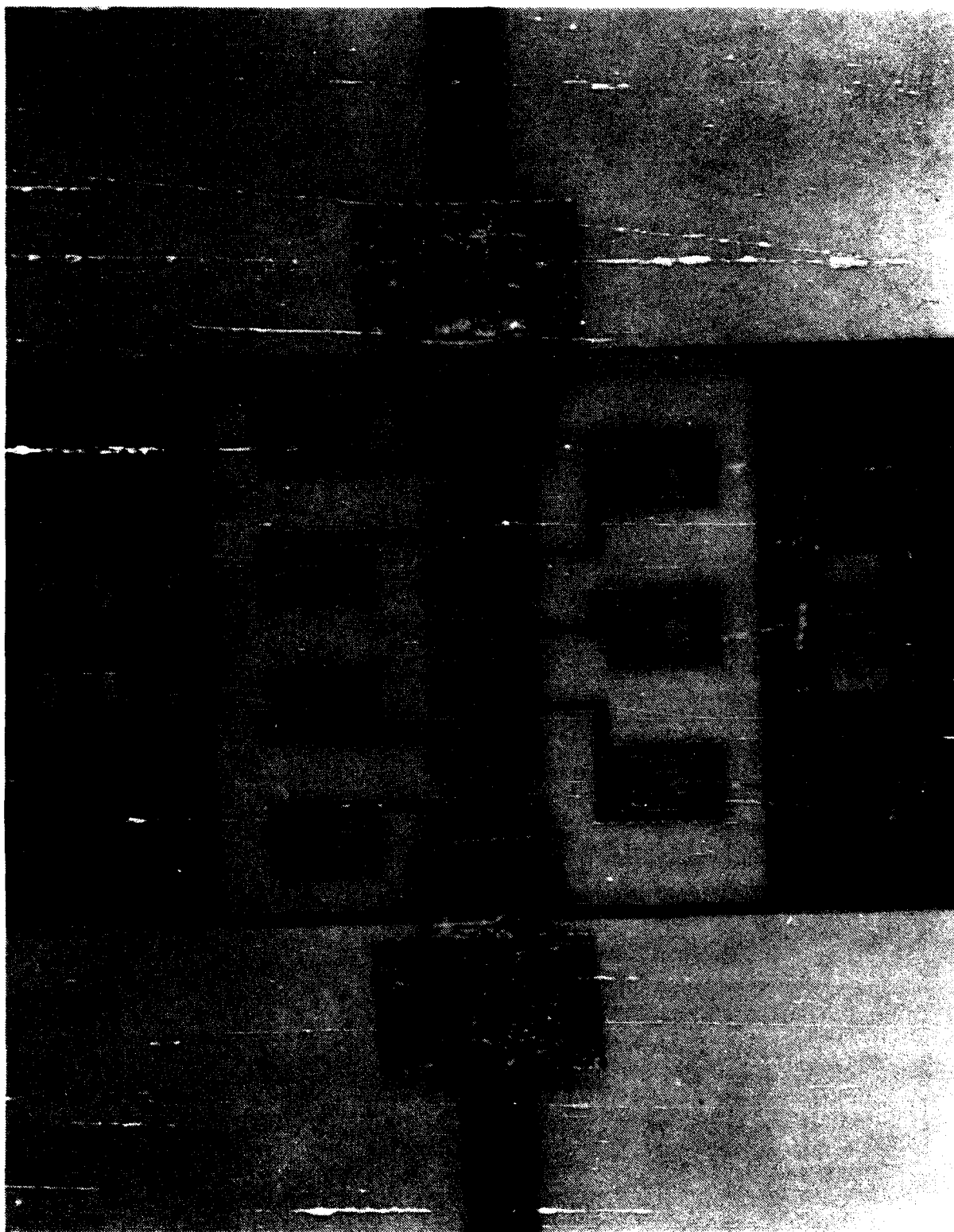


Figure 10. Earlier symmetric resonant element realization with two FETs and two varactors.

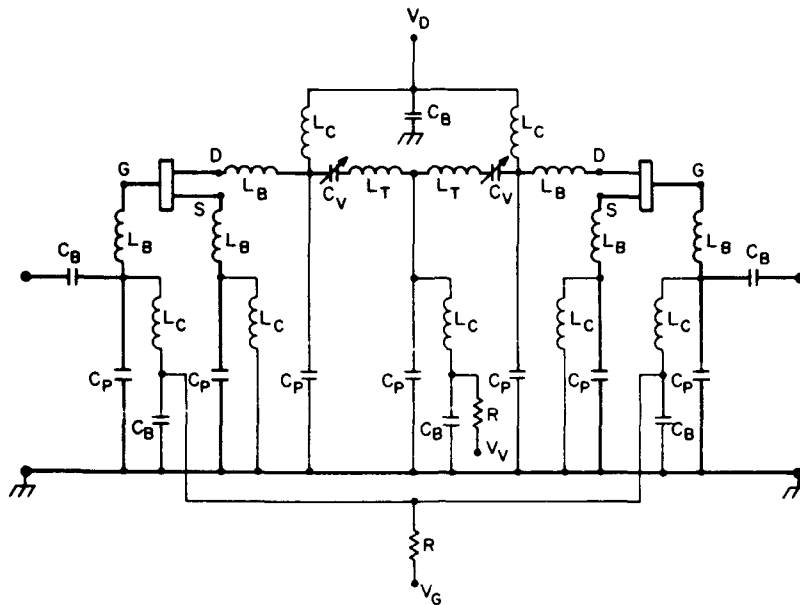
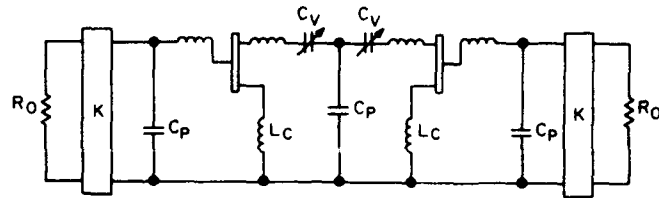


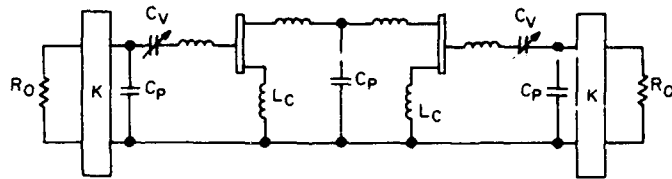
Figure 11. Equivalent circuit of symmetric element.

range, stability, and selectivity, variations in element configuration were tried. While we were able to increase stability and tuning range merely by increasing the alumina carrier height from 0.635 to 1.27 mm, we could not improve the selectivity. Thus, selectivity appears to be a function of the basic circuit configuration. Figure 12(a) depicts the original symmetric element (drain of FETs back-to-back) with the two varactors in the drain circuits of the two FETs. An element on a 1.27-mm-high carrier embedded between two impedance inverters K gave at best a tuning range of 3 GHz, and that with a relatively poor selectivity of 200 MHz at  $9 \pm 1.5$  GHz. A variation of the element with the varactors moved to the respective gate sides is shown in Fig. 12(b). This type of element caused the tuning range to be reduced to 1.8 GHz and to become a pronounced function of external loading. Also, contrary to expectations derived from calculations, selectivity did not improve.

In another element variation (see Fig. 13), the FETs are connected with gates back-to-back. Figure 13(a) shows the element with the varactors in the gate circuitry, and Fig. (13b) shows it with the varactors in the drain circuitry. The aim with this type of element was to attain greater electrical stability and increased freedom from spurious oscillations. The experimentally

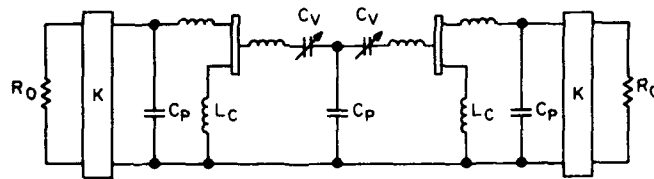


(a) TUNING IN DRAIN CIRCUIT

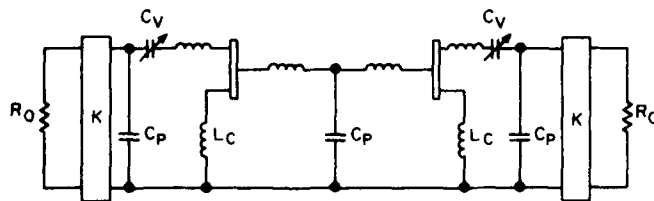


(b) TUNING IN GATE CIRCUIT

Figure 12. Symmetric element diagram of experimental single-section filter configuration (drain back to back): (a) tuning in drain circuit; (b) tuning in gate circuit.



(a) TUNING IN GATE CIRCUIT



(b) TUNING IN DRAIN CIRCUIT

Figure 13. Symmetric element diagram of experimental single-section filter configuration (gate back to back): (a) tuning in gate circuit; (b) tuning in drain circuit.

verified stability increase was offset by a poorer selectivity of 250 MHz and a smaller tuning range of 700 MHz.

The lack of selectivity of our symmetric active resonant element in actual filter configurations with inverter circuitry prompted a detailed study of the problem. The primary function of the inverter circuitry is to control the external loading of the resonator caused by terminations and/or adjacent resonators. We found that, as configured, the resonator alone is a detriment to the transformation. The FET circuitry acts as a complex impedance inverter, as shown in Fig. 9(b), in which  $R$  is a negative resistance. The magnitude of the resistance is not negligible with respect to the FET reactance, and the transformed reactive series component cannot be neglected either when compared to the reactance of the varactor. The selectivity response under these conditions is highly frequency-dependent and asymmetric.

Prevention of these undesirable effects relies upon low carrier parasitics to decouple the negative-resistance element from the common ground of the inverter circuitry. A different approach, as discussed previously in Section II.B.1.c, was used to separate the grounds of the inverters and the negative-resistance circuitry.

The element configuration finally used is shown in Fig. 7. This realization provides good electrical symmetry and requires only one FET and one varactor per element. A true series resonance is established when one considers that the parasitic pad capacitances  $C_2$  of the carrier can be absorbed by necessary inverters. The negative-resistance element between the terminals B and C in the diagram was realized electrically, as shown in Fig. 4 and described in Section II.B.1.b. A 0.38-mm-thick, 5-mm x 5-mm alumina substrate was chosen as the carrier material. Metallic thin-film technology was used to print onto the carrier the supporting pads for the varactor, the FET circuitry, high-impedance choke lines, and rf decoupling resistors. The photograph in Fig. 14 shows a close-up of the circuitry with components mounted. The FET and varactor circuitry is shielded from ground by the mounting pads. With the carrier and rf bypass capacitors attached to a 10-mm x 5-mm x 1.5-mm flange, as shown in Fig. 15, the assembly represents the basic filter building block in modular form.

#### D. EXPERIMENTAL ELEMENT EVALUATION

During the program, various aspects of element and/or filter performance were evaluated. The photograph in Fig. 16 shows a fixture in which individual

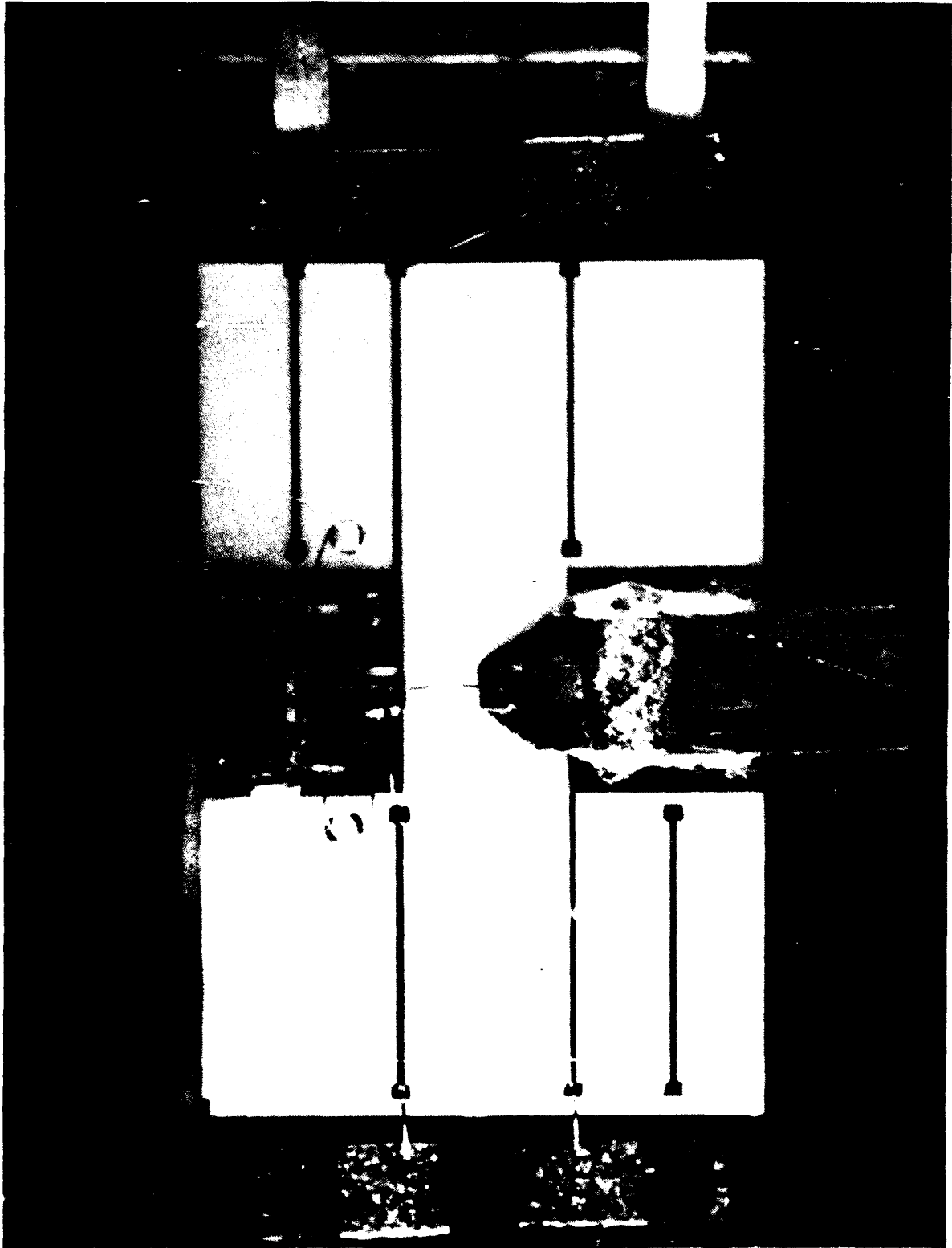


Figure 14. Photographic close-up of final element circuit with one FET and one varactor.

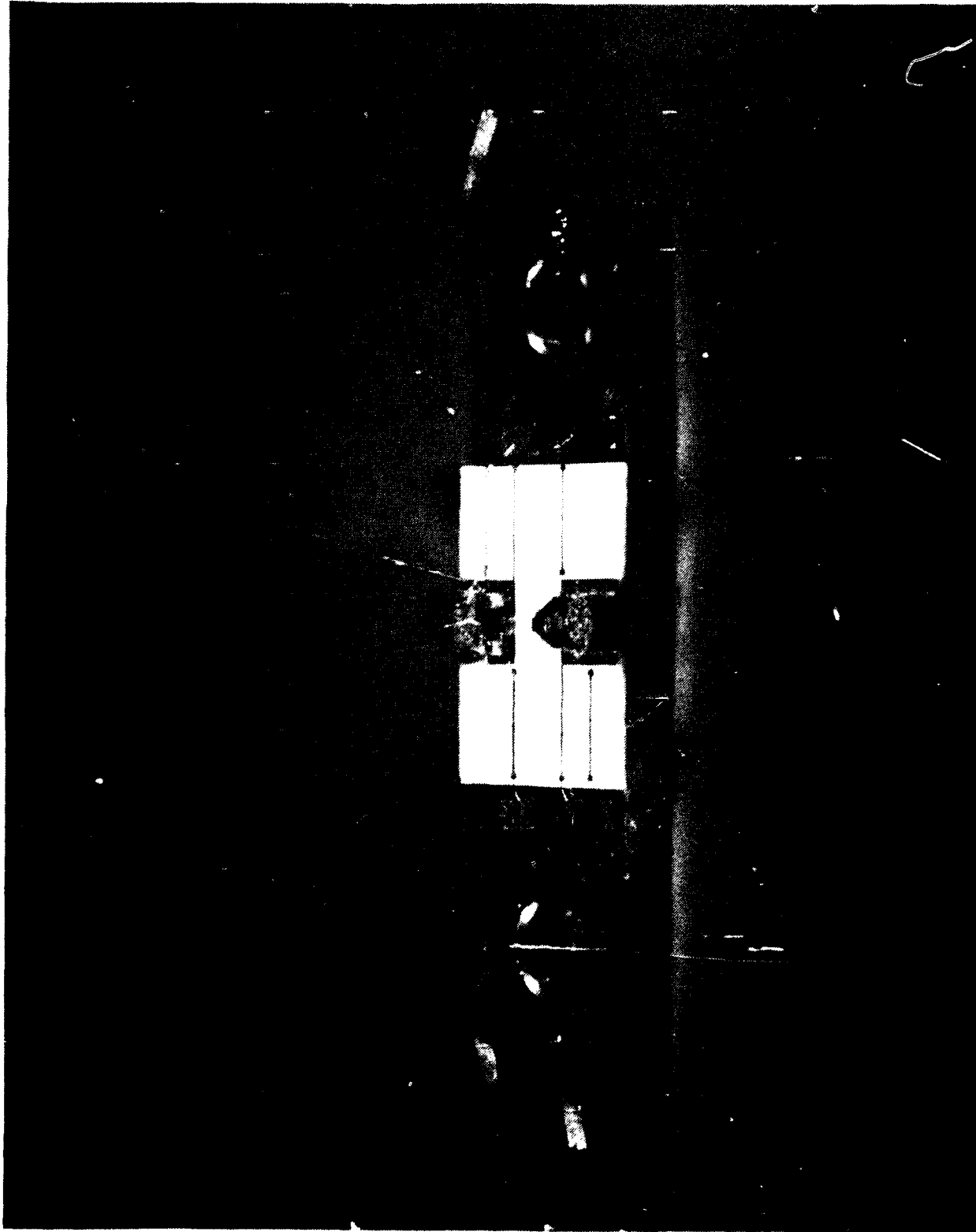


Figure 15. Resonant element module.

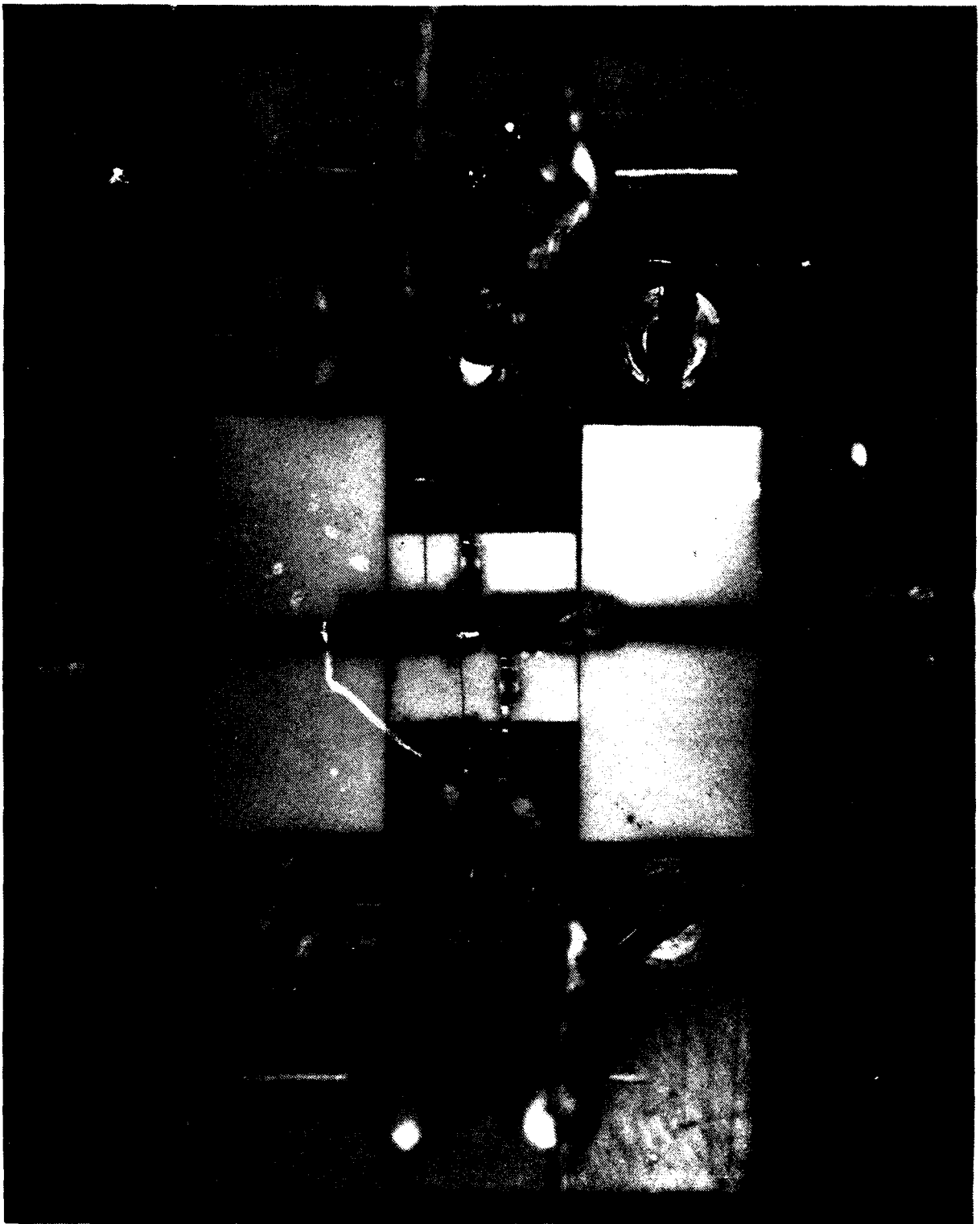


Figure 16. Test fixture for resonant element evaluation.

elements were tested. This fixture contains two 50- $\Omega$  line sections terminated by SMA-type connectors. The element is capacitively coupled to these lines via adjustable tabs. Required dc voltages for varactor and FET of the element are accessible over standoffs. Transmission and reflection responses of the element are evaluated in a manual test setup as shown in Fig. 17. This setup permits single and swept frequency filter evaluation at fixed and leveled input powers. Single-frequency measurements with counter accuracies (less than 30 Hz) are made possible by both the "lockbox" feature of the counter used (EIP 371) and the FM capability of the signal generator (HP 8620C). In this paragraph the results of individual evaluation aspects are highlighted.

### 1. Selectivity

The selectivity of a bandpass filter is defined by the 3-dB bandwidth and the transmission rejection as a function of frequency. The rejection is mainly determined by the basic filter design (number of elements, response shaping, etc.) which, in this case, is that of a single-section, maximally flat filter. The 3-dB bandwidth, on the other hand, is a function of the resonator parameters (slope parameter and  $Q$ ) and the external loading (determined by the coupling). The unloaded  $Q$  of the resonator can be adjusted over a wide range with the gate voltage of the FET up to a point at which instabilities will take over. The coupling at input and output is adjustable via the proximity capacitance between the gap of a tab, which extends from each end of the resonator, and the printed conductor of the 50- $\Omega$  line sections. This range of adjustment is also limited by stability considerations. Figure 18 shows the measured results for an element with coupling adjusted to assure stability while maintaining a 0-dB transmission loss over the tuning range. The 3-dB bandwidth, voltage standing-wave ratio (VSWR), and gate and varactor voltages are shown as a function of midband frequency. The frequency is adjusted by varying the varactor voltage while at each setting the gate voltage is adjusted to result in a 0-dB transmission loss. The high degree of uniformity of the 3-dB bandwidth ( $21 \pm 1$  MHz) over a 2300-MHz tuning range is not typical, but demonstrates ultimate feasibility. Typical reproducible minimum values of bandwidth at present lie between 20 and 40 MHz, attainable over the entire 0- to 30-V tuning range.

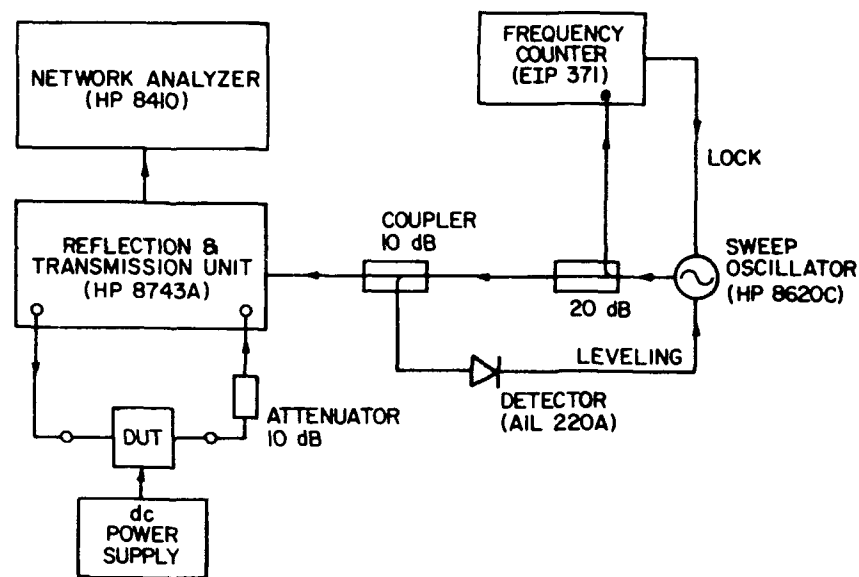


Figure 17. Manual network analyzer test setup for transmission and reflection evaluation.

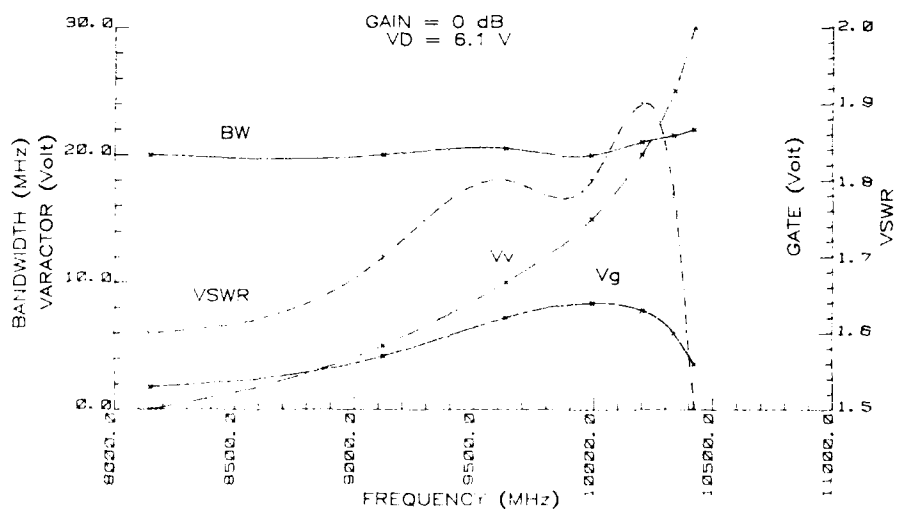


Figure 18. Measured 3-dB bandwidth and VSWR vs midband frequency of single-section filter with high selectivity and small bandwidth deviation over tuning band.

## 2. Tuning Range

The tuning range is a function of the capacitance ratio of the varactor between useful minimum and maximum varactor voltage limits and of other capacitive reactances in the resonator proper that affect this ratio. These unwanted but unavoidable reactances are introduced by the carrier, the interconnections between components, and the FET circuitry; they effectively reduce the capacitance ratio and, with it, the tuning range. A varactor with high cutoff frequency (high-Q) and large capacitance ratio is best suited for broadband tuning. The reactance of such varactors is high, and the series resistance is low.

Although the varactor and the FET chosen during this program were not fully optimized, the maximum frequency tuning range for the particular combination was found to extend over  $2.5 \pm 0.1$  GHz, while assuring stability and adequate selectivity (30-60 MHz). In order to demonstrate wider-band tuning, the varactor reactance was doubled by connecting two varactors in series. With the FET circuit unchanged, the tuning range of such a combination increases because of the smaller reactive loading effect of the FET on the varactor reactance. The observed tuning range increased from 2.4 to 3.5 GHz. However, since the series resistance of the varactor combination also doubled, the negative resistance of the FET was not sufficient to maintain good selectivity over the full varactor tuning range. Attempts to increase the negative resistance via gate voltage adjustments were fruitless since instabilities near the upper frequency limit occurred.

The plot in Fig. 19 shows the varactor and gate voltages at the corresponding frequencies (note the 0- to 60-V range necessary to drive the series combination of two 30-V varactors). Figure 20 shows gain and 3-dB bandwidth vs frequency. Selectivity decreases rapidly as transmission loss increases because resonator Q decreases as a result of insufficient negative resistance. Figure 21 shows the VSWR; as the gain deteriorates, so does the VSWR because of mismatches caused by the unchanged coupling structure. It is recommended that, in future phases of the program, the varactor-FET combination be optimized so that simultaneous attainment of large tuning bandwidth and high selectivity is possible.

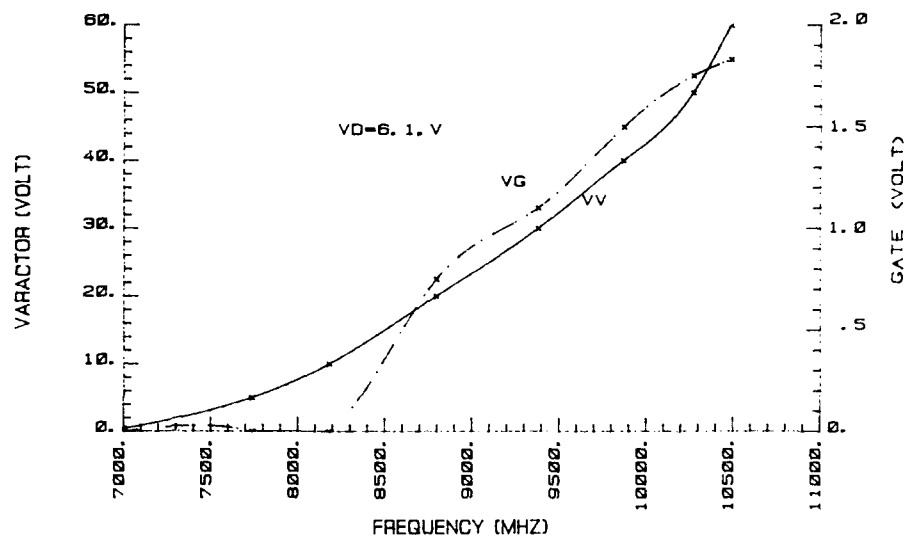


Figure 19. Varactor and gate voltages vs midband frequency in broadband tuning experiment with two varactors in series.

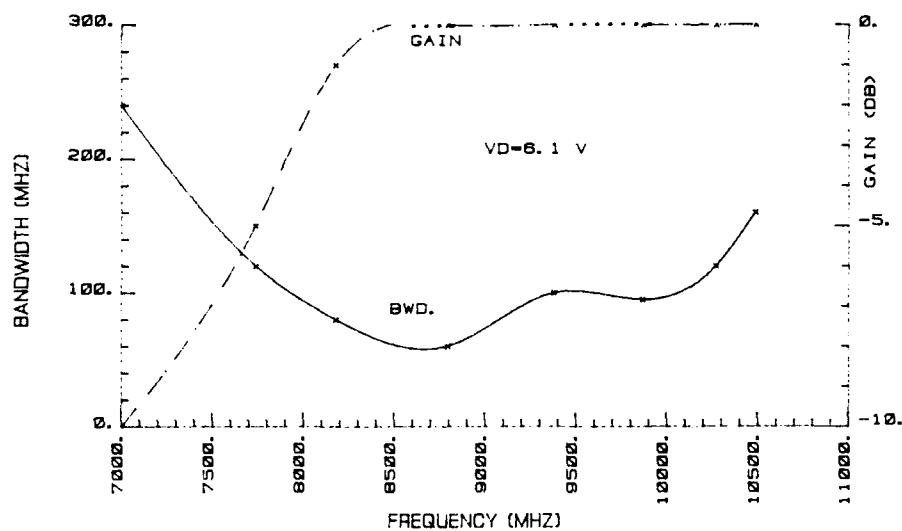


Figure 20. Measured 3-dB bandwidth and transmission gain vs midband frequency (broadband experiment).

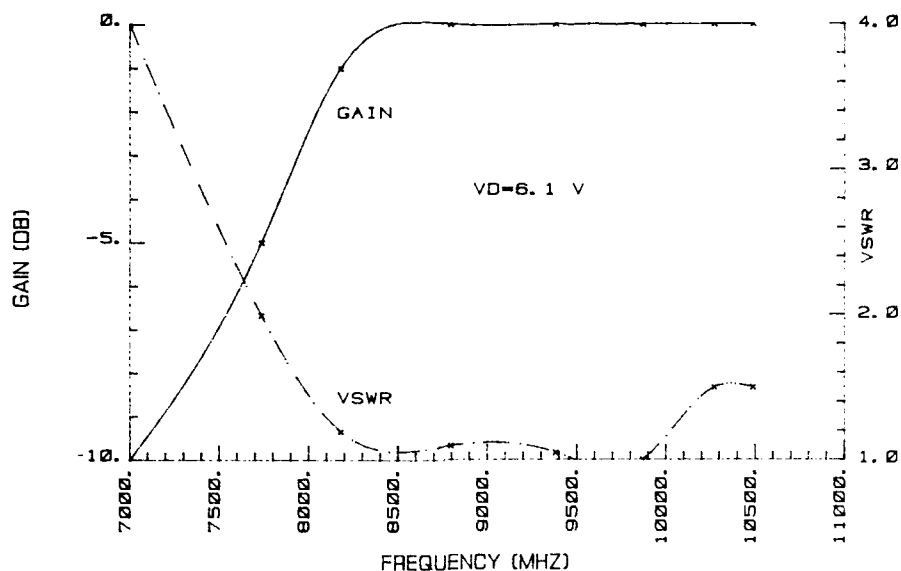


Figure 21. Measured VSWR and transmission gain (broadband experiment).

### 3. Signal Input Effects

During earlier efforts (Phase I and Phase II, Task 1), it was already observed that power input affects the filter response. Generally the transmitted power is reduced, and midband frequency shifts as input power is increased. Whereas gain reductions of a fraction of a decibel can be observed with power inputs as low as -15 dBm, noticeable frequency shifts of a few megahertz occur at the -10-dBm level. As it was also observed, the effect is a function of element loading; we therefore suspect that the rectified rf voltage at the gate junction of the FET is producing power-dependent variations of negative resistance as well as a reactance sufficient to cause the changes observed in selectivity and transmission. The plot in Fig. 22 shows the response, evaluated on an automatic network analyzer, of a tightly coupled element (with 95-MHz bandwidth) for three different power input levels. For a 20-dB input level change from -30 to -10 dBm, the center frequency shifts by less than 10 MHz, the midband loss increases by 1.2 dB, and the 3-dB bandwidth increases by 5 MHz (from 95 to 100 MHz). At higher selectivity adjustments (~20 MHz bandwidth), frequency shifts can also be as large as 10 MHz, while loss can increase by 4 dB, and bandwidth by 20 MHz.

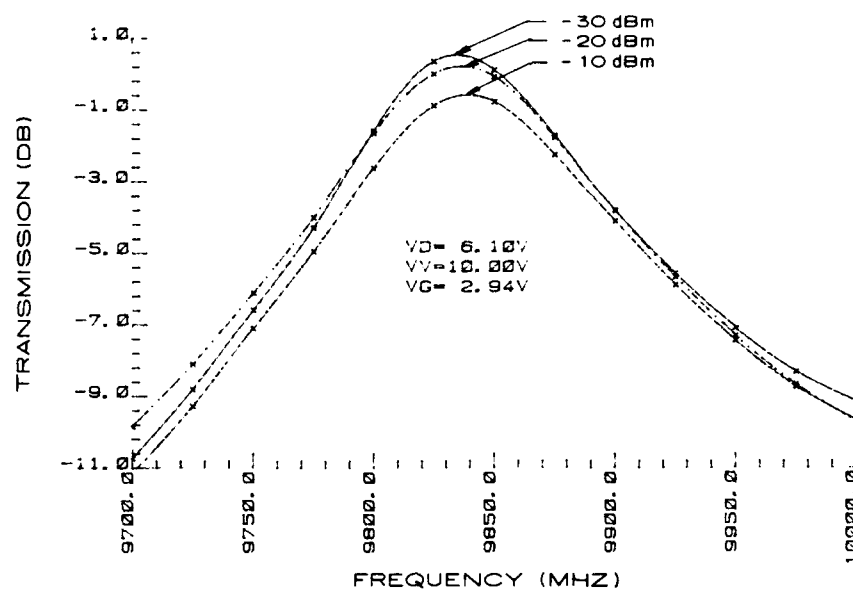


Figure 22. Measured transmission passband response at a given filter setting for three different input power levels.

The effects on filter performance of power input from two signals were briefly observed. In the evaluation, the test setup shown in Fig. 23 was used. Two signals, adjustable in frequency and amplitude, were applied over a 3-dB hybrid coupler to the input of the filter. The rf output of the filter was observed on a spectrum analyzer. Amplitude responses of each signal within and outside of the passband of the filter, amplitude and frequency of signals generated by FET nonlinearities, could be determined. The filter was adjusted with voltages as shown in Fig. 22. The observed amplitude and frequency shifts were about the same for a combined power input of the two signals within the passband as were those observed above for a single signal. The third-order intermodulation (IMD) for two equal-amplitude signals in the passband ( $\Delta f = 15$  MHz) as a function of the power input of each signal is shown in Fig. 24. The IMD product decreased while one signal remained in the passband and the difference frequency was increased. The power input of the second signal at the response skirts was also increased to give identical power outputs of the two signals; with a signal separation of 200 MHz, no third-order distortions were observed when the inband signal was -27 dBm and the out-of-band signal +6 dBm. However, as total power output of the two signals was increased, response shifts were about the same as for a single signal at a comparable power output.

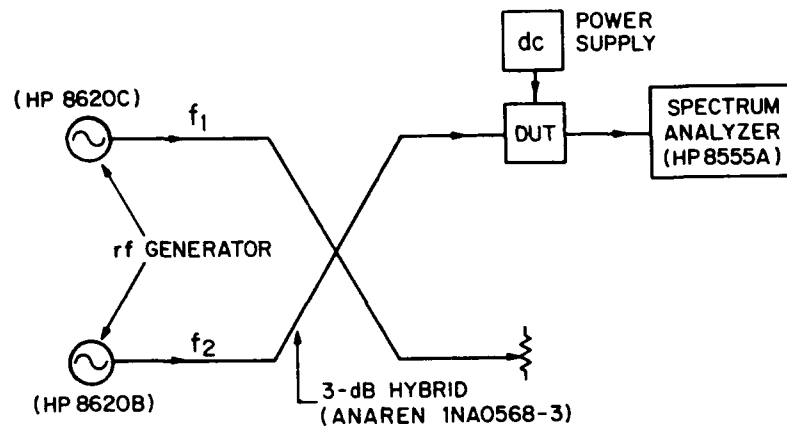


Figure 23. Test setup to evaluate IMD and other two-signal effects.

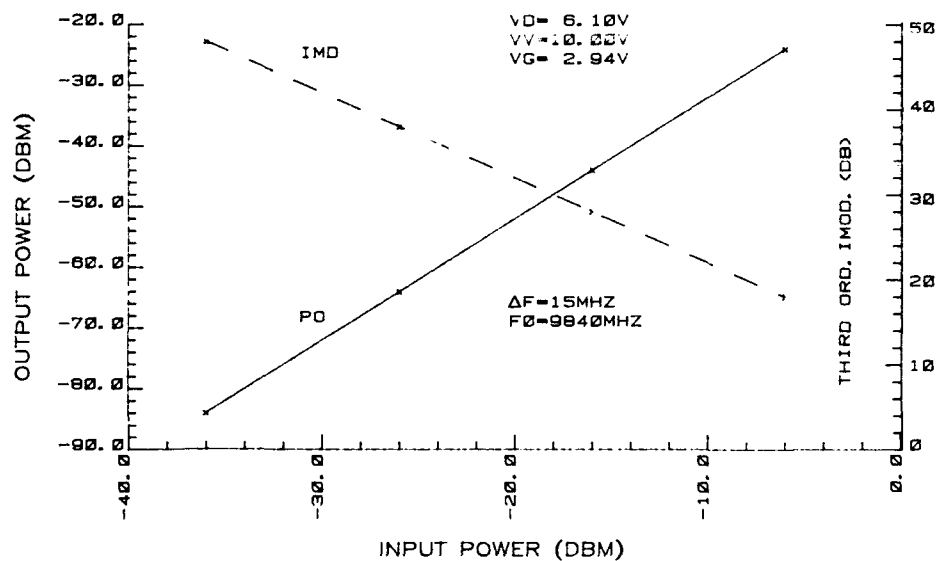


Figure 24. Measured two-signal intermodulation distortion (absolute and relative) as a function of input power level.

#### 4. Noise Figure

Transmission loss is not the limiting parameter of noise figure in active-filter applications; the filter loss is generally negligible or, with some operating voltage adjustments, can turn into gain. As with other active components,

output noise is a disturbing factor and noise figure is an appropriate measure of performance. The noise figure is increasingly important in high-sensitivity applications and those requiring large dynamic ranges. The plot in Fig. 25 shows the measured noise figure of a single-section filter over the 8.9- to 10.4-GHz frequency range. This noise figure was evaluated at discrete frequencies in a test set shown in Fig. 26. The isolator between mixer and filter to be tested is essential since it prevents local oscillator leakage from reaching the filter; erroneous noise figure readings were observed without this isolator. At each measured spot frequency, the filter was adjusted for a 0-dB transmission loss. The measured 16- to 20-dB noise figure is typical and conforms to values obtained at earlier phases of this program. The relatively large values of noise figure were neither expected nor fully understood. We expected the noise figure to be somewhat larger than that for an amplifier with the same FET, which is rated 4 dB at 10 GHz, since the FET loading is far from the optimum noise impedance values. The feedback configuration must be responsible for a large portion of the noise figure. Future studies on noise limitations and noise figure reductions are recommended.

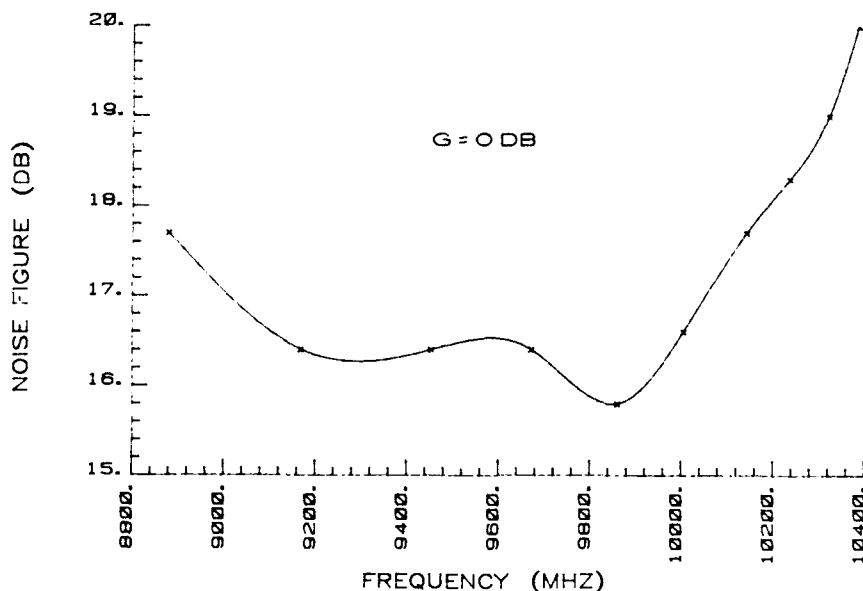


Figure 25. Measured noise figure at different frequency settings.

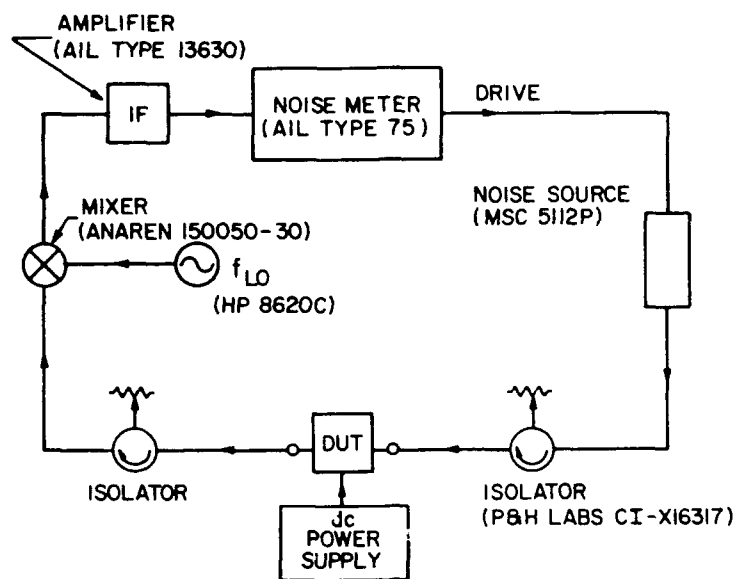


Figure 26. Noise figure test setup.

## 5. Temperature Effects

The major effects of temperature on filter performance are caused by the temperature sensitivity of the varactor and the FET. This sensitivity changes the reactances and the negative resistance within the resonators. These effects were already observed and reported during the Task 1 efforts of this program [2]. Similar results were observed on an element evaluated during this task and are shown in Fig. 27. With the operating voltages and the rf drive level kept constant, and the temperature varied between 10 and 50°C, the center frequency decreased by about 930 kHz per degree Celsius; the 3-dB bandwidth increased by 1.1 MHz per degree Celsius. The midband transmission decreased by nearly 0.2 dB per degree Celsius at the higher test temperatures, and about 0.75 dB per degree Celsius at the lower temperatures. These relatively large changes with temperature suggest the use of either oven-controlled operation or voltage control to compensate partially for these changes.

## 6. Tuning Speed

The tuning operation of the filter type developed during this program depends on accurate tuning voltage settings for attaining a predetermined response at a predetermined frequency. The number of variable voltages in the

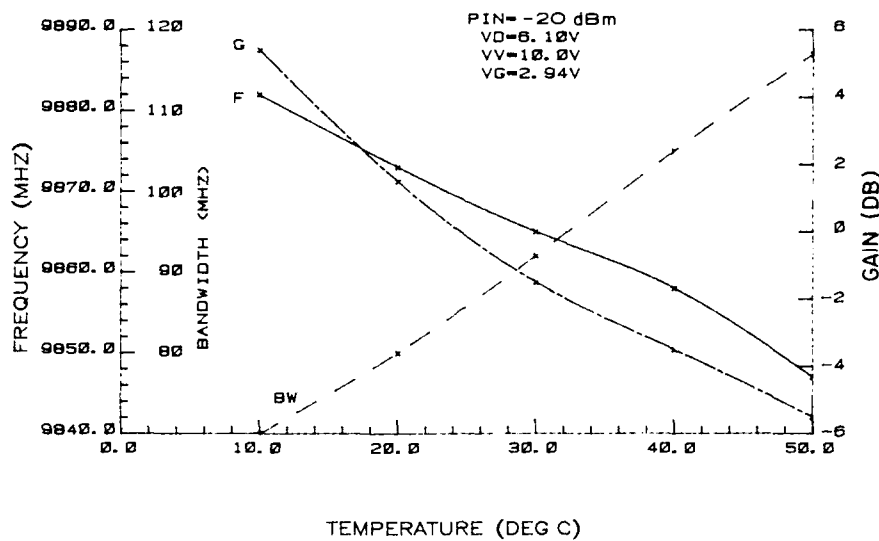


Figure 27. Measured effects of temperature upon 3-dB bandwidth, midband frequency, and transmission gain.

worst case are  $2N$ , where  $N$  is the number of elements in the filter. It is envisioned that some of the voltages can be derived from a common variable, one that is attainable under microprocessor control and uses preprogrammed voltage look-up tables. This microprocessed addressing system activates the appropriate driving circuitry for the filter. The tuning speed of the filter is a combination of addressing system access time, slewing and settling times of the driving system, and the time constants of the varactor and gate circuitry. Since the time constants in the experimental element are only about 100 ns, the ultimate speed of the operational filter will be determined mainly by the addressing and driving circuitry. If need be, the 100-ns time constants could be further reduced by altering the decoupling resistors in the dc lines and by reducing the values of the feedthrough capacitors.

The tuning speed can be evaluated in a test set shown in Fig. 28. Two different cw signals within the tuning bandwidth of the filter are injected into the filter input over a 3-dB hybrid. The filter operating voltages, which correspond to passband responses at the two injected frequencies, are provided by the two levels of a zero-offset pulse. The detected output of the filter together with the driving pulse are observed on a dual-trace oscilloscope. The filter response time is estimated by the difference between the drive rise time

and the time the detected output has settled. A single-section test filter was evaluated in such a test set. The two frequencies were separated by 180 MHz ( $f_1 = 9.87$  GHz,  $f_2 = 10.05$  GHz). The drive pulse in our experiment exhibited a leading- and trailing-edge ringing of about 200 ns, making speed evaluations inaccurate. Excluding this ringing we estimated the filter to respond in less than 200 ns.

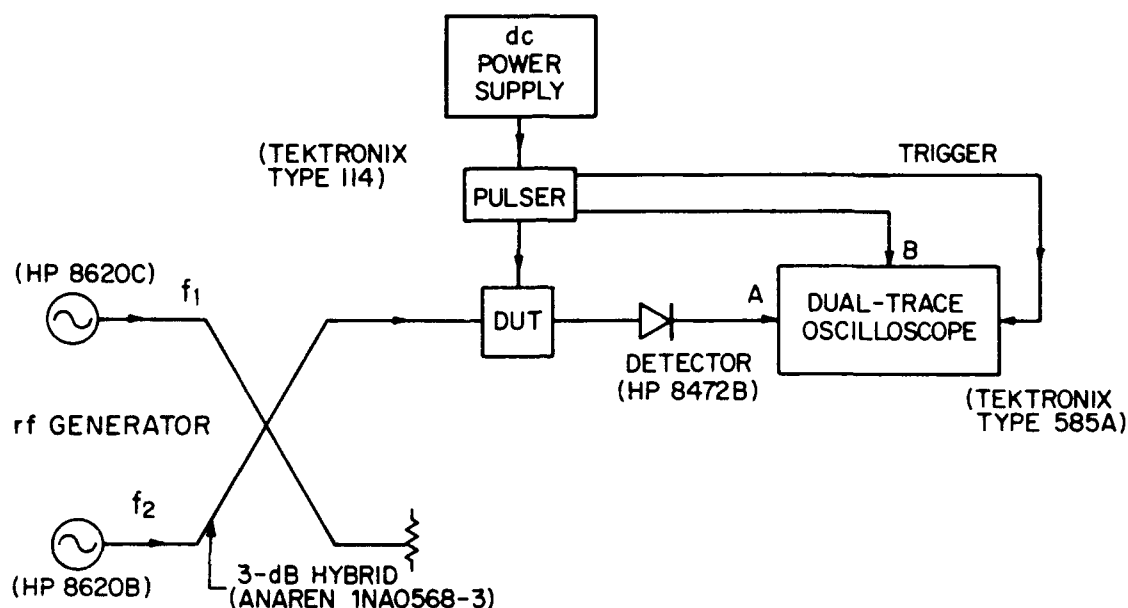


Figure 28. Test setup to evaluate filter tuning speed.

## E. PROTOTYPE FILTERS

The step-by-step development of the filter element described in the above sections led to an element design that promises a high degree of success to meet program objectives of extended filter-tuning bandwidth. The particular design was frozen at some time into the program to allow ample time for multi-section design, experimentation, and evaluation. Some of the experimental data that demonstrate electrical element symmetry with high selectivity (Section II.E.1) and freedom of element detuning effects in a two-section-filter design (Section II.E.2) are shown below. These two characteristics were lacking in previous element designs in both Task 1 and earlier Task 2 efforts.

## 1. Single-Section Filter

The test fixture used to evaluate single-section-filter performance is shown in Fig. 29. The sequence of plots in Figs. 30 through 37 summarizes the performance of an element in such a single-section-filter configuration. The input and output coupling was adjusted to give, at each varactor voltage setting a response with about 60-MHz bandwidth, while the gate voltage was adjusted for 0-dB transmission loss. Shown in these plots for each frequency setting are the required voltages (Fig. 30), the 3-dB bandwidth (Fig. 31), and the input and output VSWR (Fig. 32). The responses for five particular varactor voltage settings (Figs. 33-37) were obtained by use of an automatic network analyzer. The results demonstrate nearly ideal one-section-filter responses with loaded  $Q$ -values of about 130 over a 1.4-GHz tuning range, while input and output matches stay below a VSWR of 1.7:1. The plots in Figs. 38 and 39 demonstrate symmetry with respect to power flow and show the forward and reverse transmission responses and reflection coefficients for a particular filter adjustment.

When a different element was adjusted for higher selectivity (3-dB bandwidth of 23 MHz), the results with respect to symmetry were similar. The plot in Fig. 40 shows the amplitude response, Fig. 41 the phase response, Fig. 42 the group delay, and Fig. 43 the VSWR of this filter. The phase and delay responses are also as expected for a maximally flat single-section filter.

## 2. Two-Section Filter

Two experimental elements were arranged within a metallic enclosure for two-section-filter operation. The photograph of Fig. 44 shows the two elements, capacitively coupled to two 50- $\Omega$  microstrip line sections that lead to the input and output terminations, and the capacitive coupling between elements. Most of the area within the enclosure is taken up by the two substrates for the connecting lines. The coupling was adjusted by observing the skirt selectivity, bandwidth, and input and output match while maintaining a true two-section response.

The attainable tuning bandwidth and absolute frequencies were entirely determined by the performance of the single elements. The tuning bandwidth of the filter is equal to the largest common frequency range of the two elements. This range for the particular elements is indicated by dashed vertical lines in Fig. 45, which shows at each frequency the necessary four voltages to obtain a

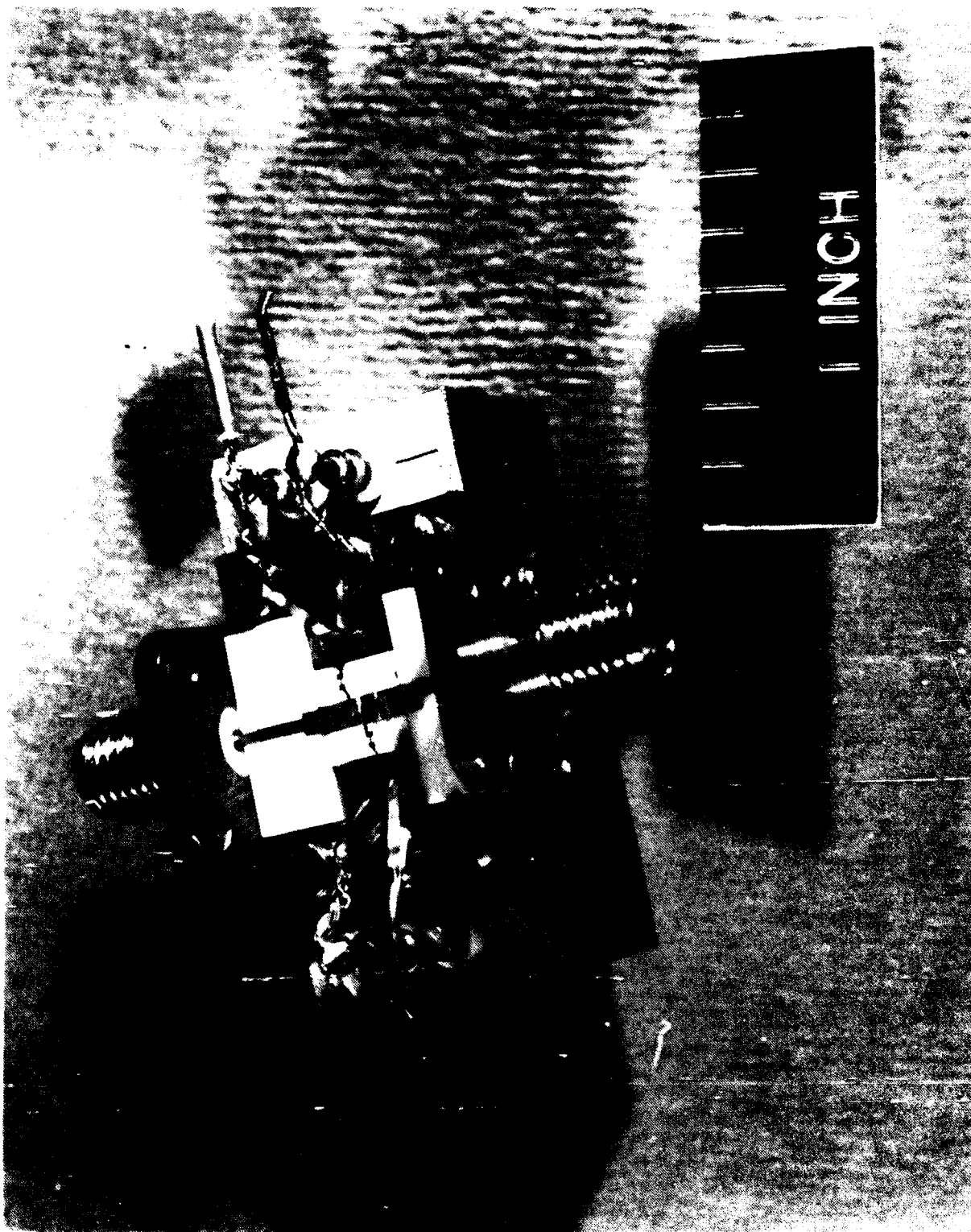


Figure 29. Single-section filter prototype.

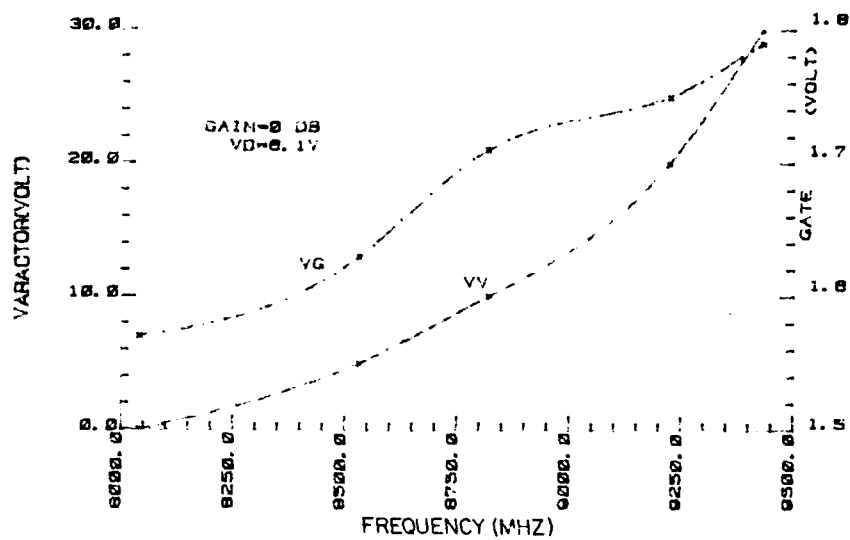


Figure 30. Varactor and gate voltage settings vs midband frequency.

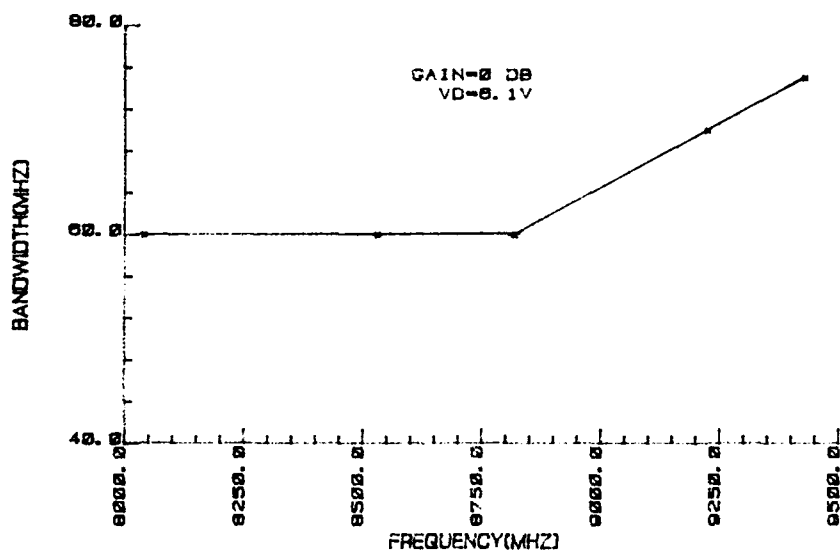


Figure 31. Measured 3-dB bandwidth vs midband frequency.

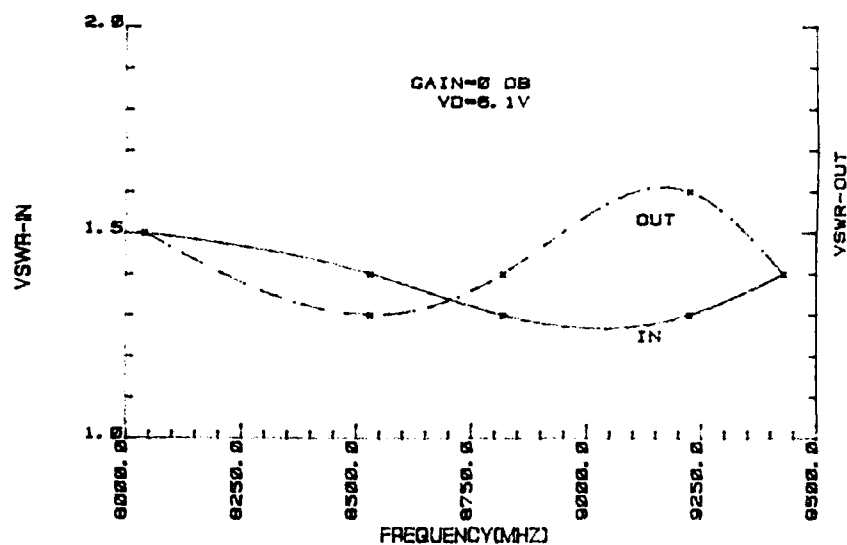


Figure 32. Measured input and output VSWR vs midband frequency.

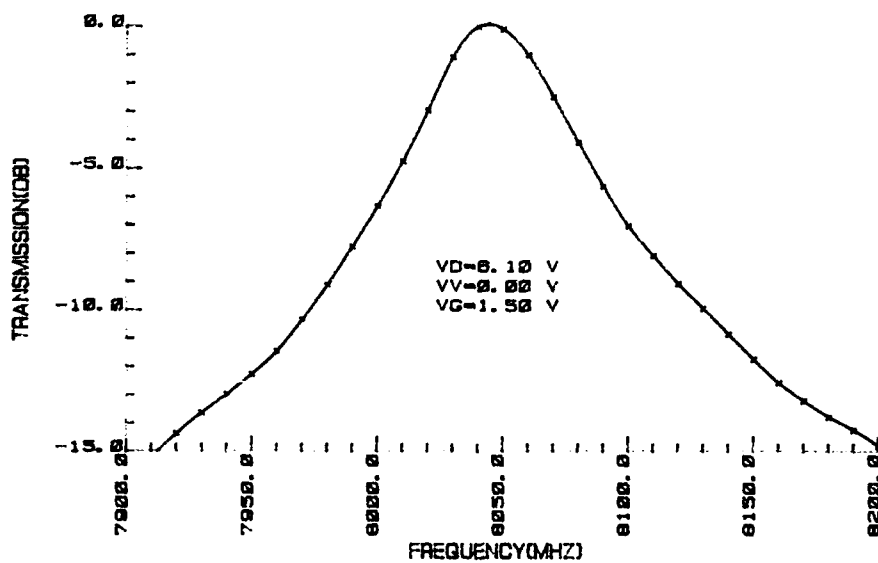


Figure 33. Measured transmission passband response of single-section filter ( $V_v = 0$  V).

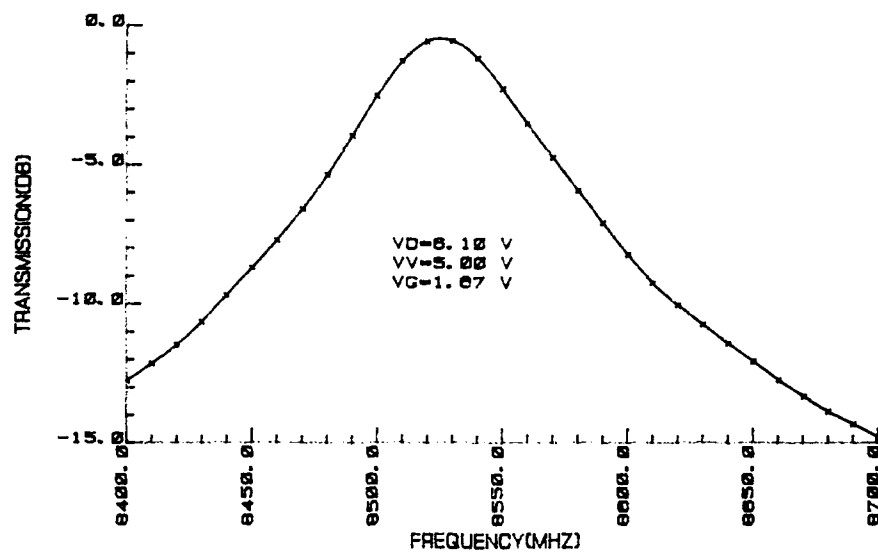


Figure 34. Measured transmission passband response of single-section filter ( $V_v = 5$  V).

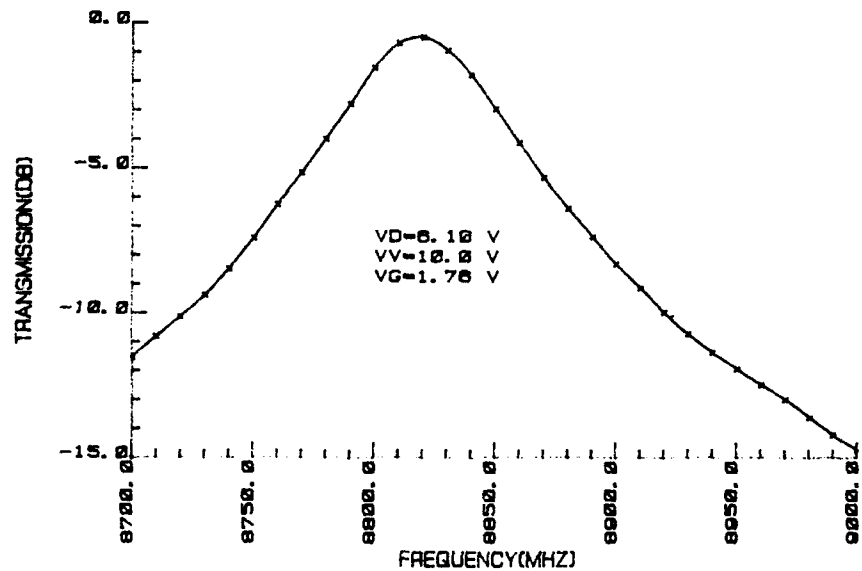


Figure 35. Measured transmission passband response of single-section filter ( $V_v = 10$  V).

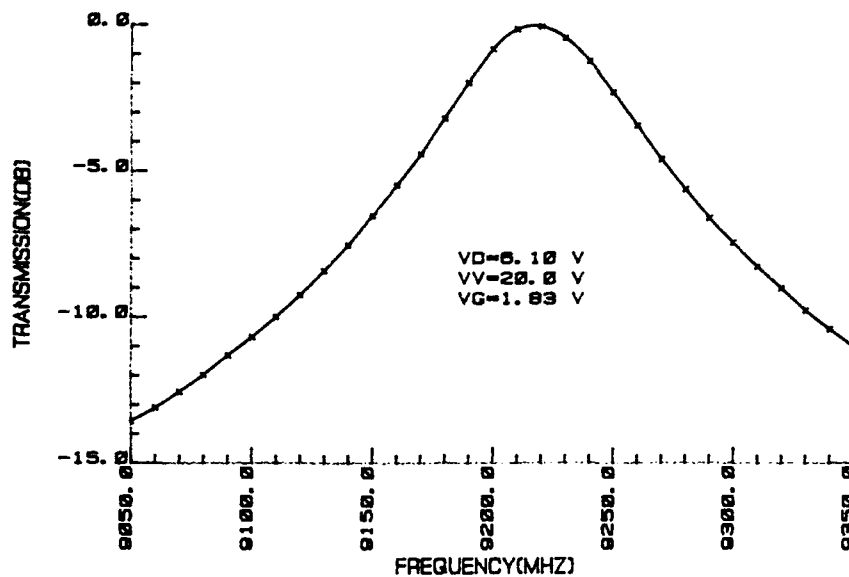


Figure 36. Measured transmission passband response of single-section filter ( $V_v = 20$  V).

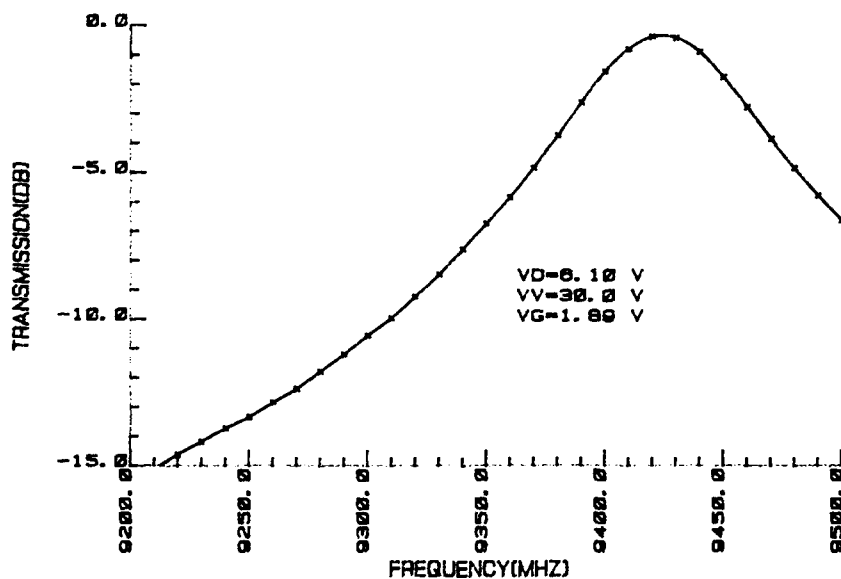


Figure 37. Measured transmission passband response of single-section filter ( $V_v = 30$  V).

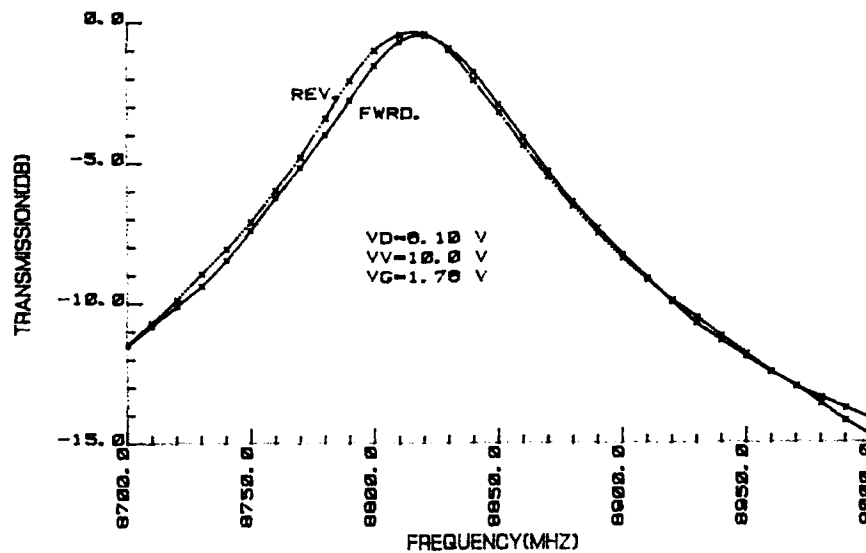


Figure 38. Measured transmission passband response of single-section filter (forward and reverse power flow).

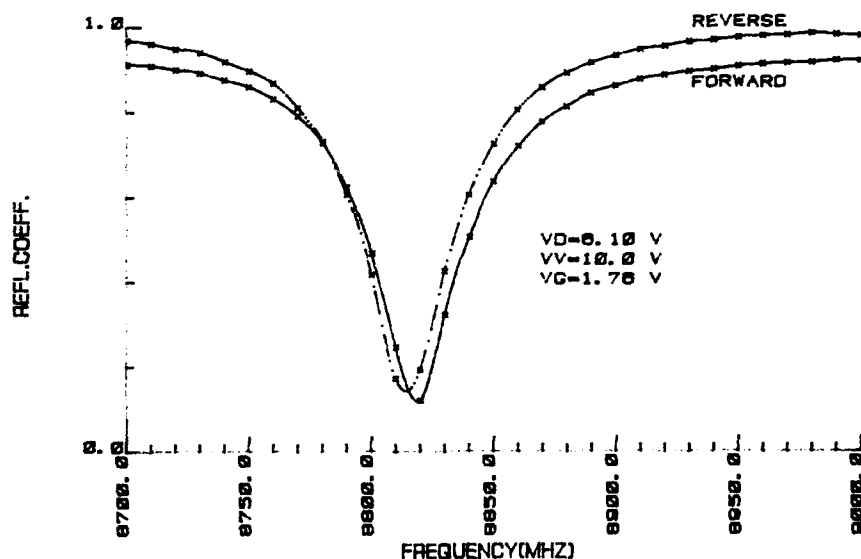


Figure 39. Measured input and output reflection coefficient in passband of single-section filter.

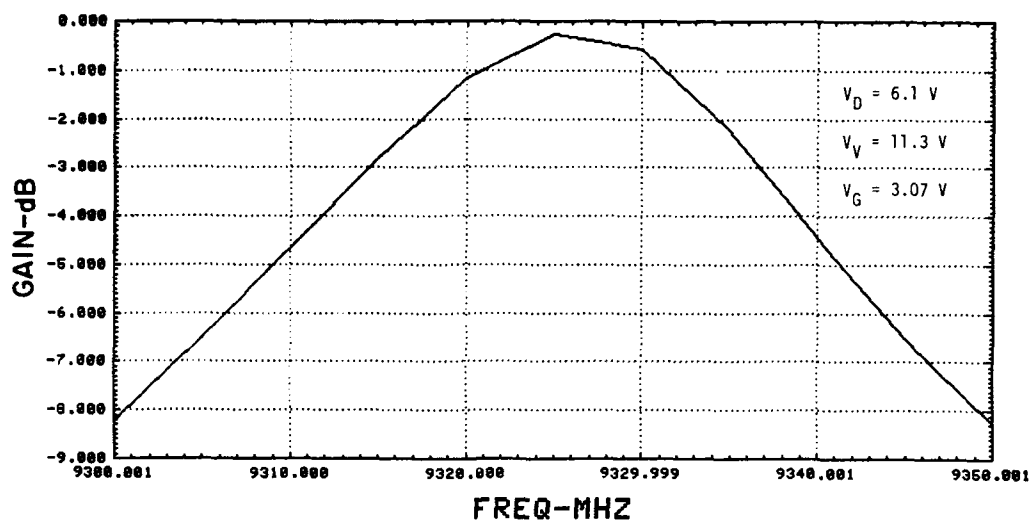


Figure 40. Measured transmission response of a single-section filter adjusted for high selectivity.

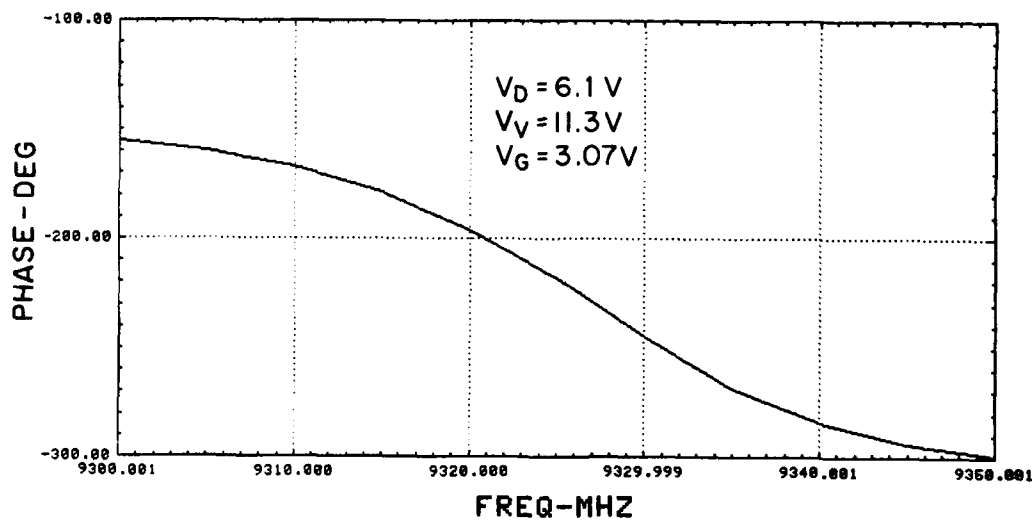


Figure 41. Measured phase response in passband of high-selectivity filter.

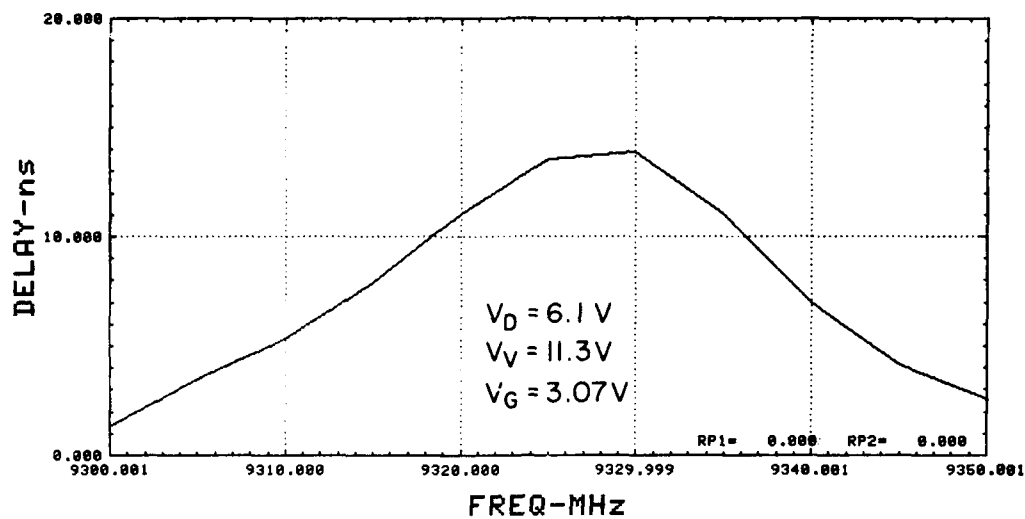


Figure 42. Measured group-delay passband response of high-selectivity filter.

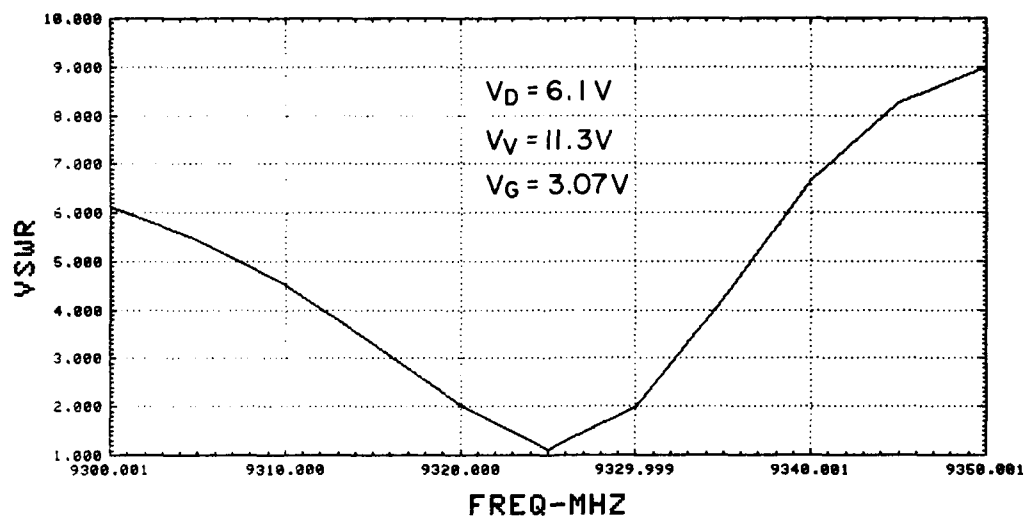


Figure 43. Measured VSWR in passband of high-selectivity filter.

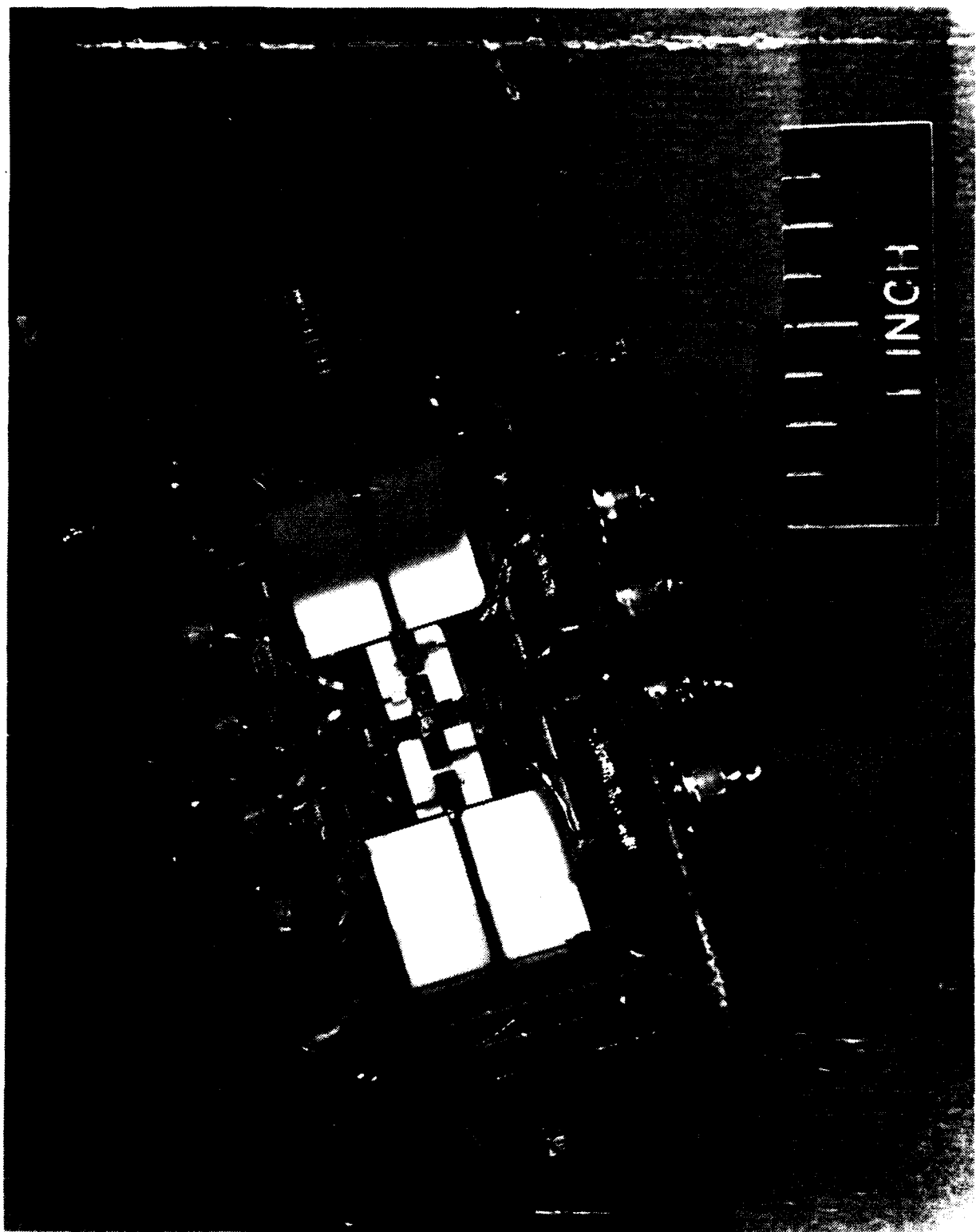


Figure 44. Two-section filter prototype.

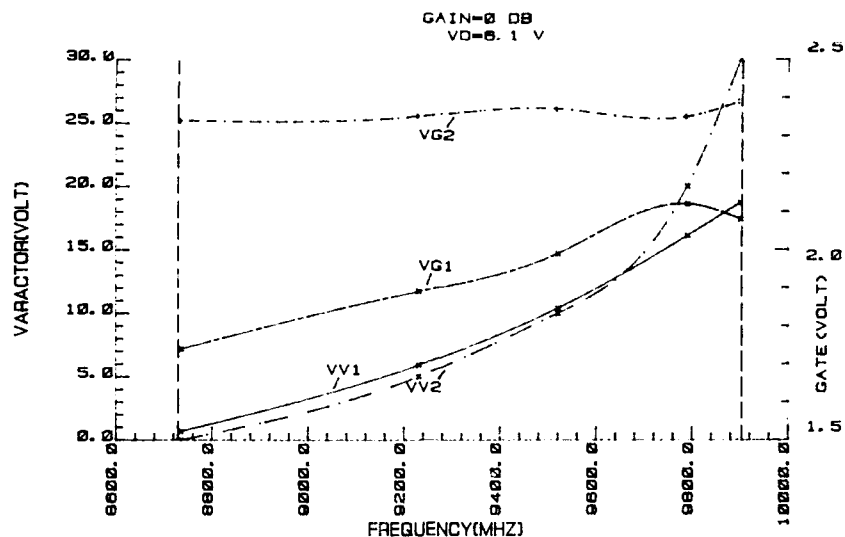


Figure 45. Varactor and gate voltage vs midband frequency of each element in two-section prototype filter.

0-dB transmission loss. Figure 46 shows the corresponding 3-dB bandwidth and the input VSWR. The symmetric nature of this filter is demonstrated via Figs. 47 and 48, which show forward and reverse characteristics of reflection coefficient and amplitude response, respectively, for a particular frequency setting.

During filter evaluation a strong resonance of the enclosure was detected at 11.8 GHz. This spurious resonance was eliminated with a layer of absorbing material in the cover. In the final filter a metallic partition was used to suppress enclosure resonances.

Control over coupling was demonstrated on a different two-section filter in which coupling was adjusted to attain a Chebyshev response. Figure 49 shows the amplitude response obtained near midband. The 3-dB bandwidth is 40 MHz, and the midband ripple is about 2 dB. In Fig. 50 the response is plotted over a larger frequency range; the increased selectivity of this type of filter over that of a maximally flat response is noticeable. The nonlinear phase associated with Chebyshev responses is evident in Fig. 51. The measured group delay and return loss are shown in Figs. 52 and 53, respectively.

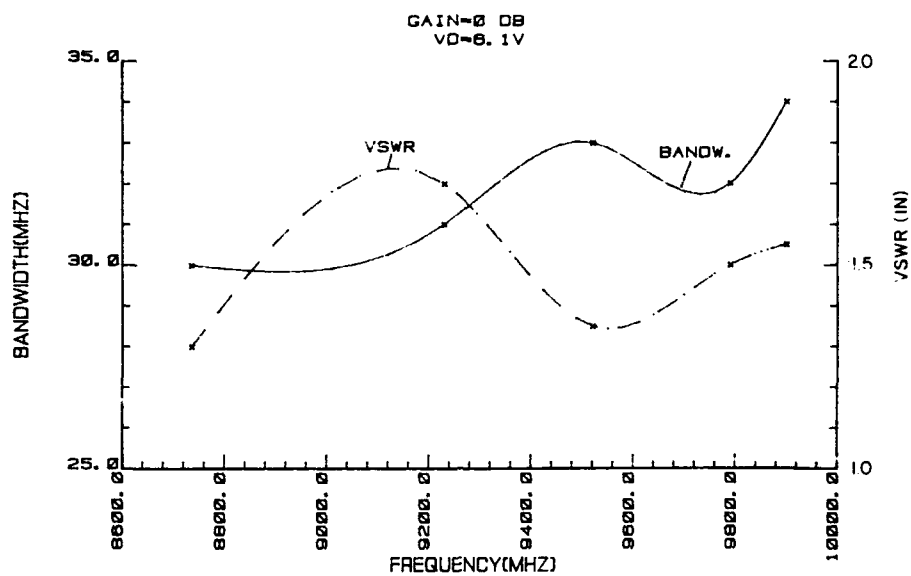


Figure 46. Measured 3-dB bandwidth and VSWR vs midband frequency of two-section prototype filter.

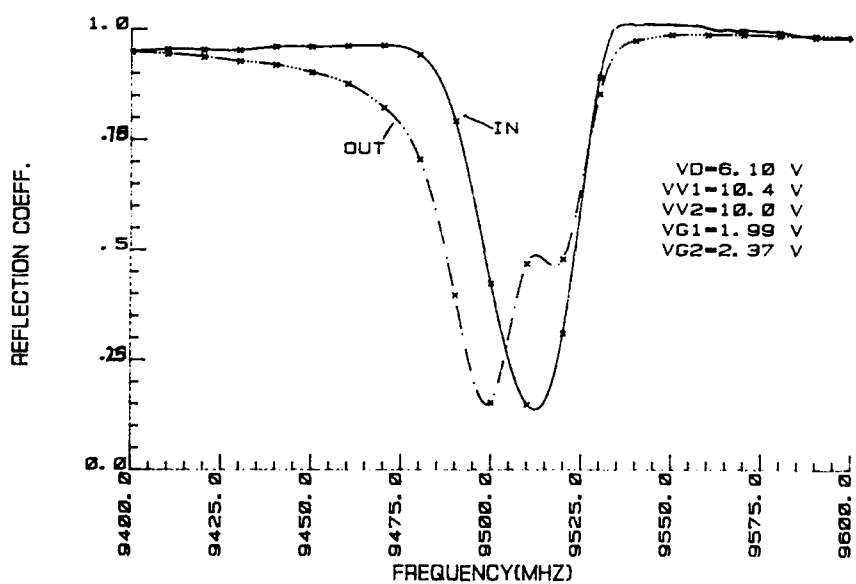


Figure 47. Measured input and output reflection coefficient passband response of two-section prototype filter.

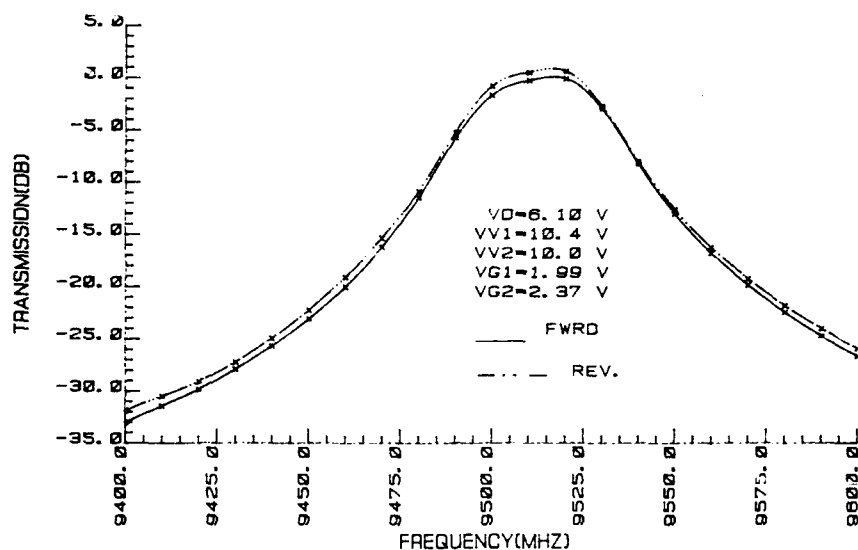


Figure 48. Measured transmission passband response for forward and reverse power flow of two-section prototype filter.

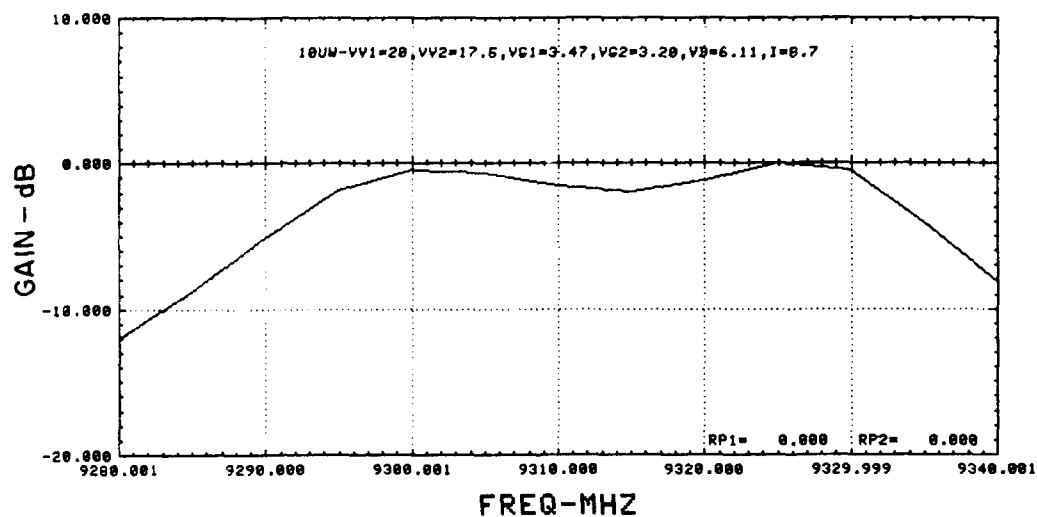


Figure 49. Measured passband response of experimental filter with Chebyshev response.

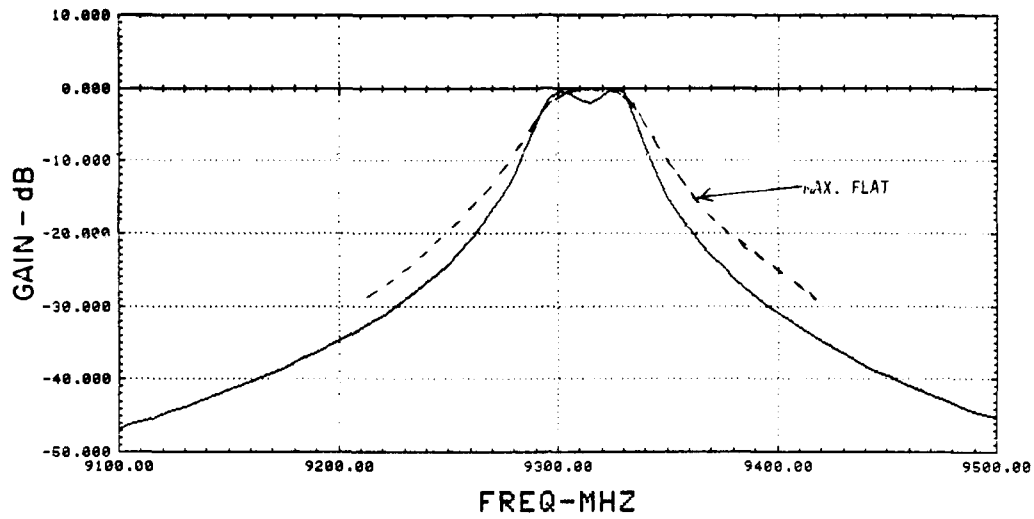


Figure 50. Measured selectivity of experimental two-section filter with Chebyshev response.

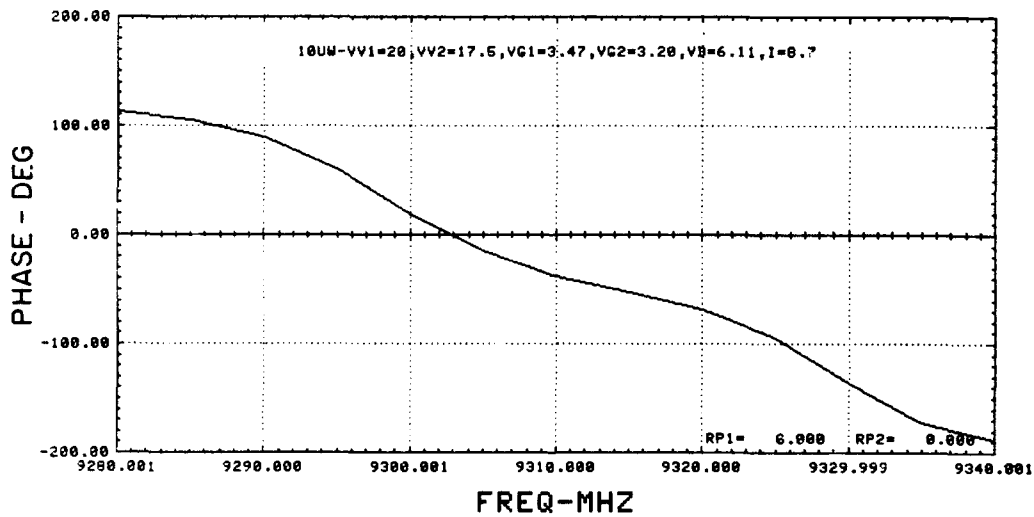


Figure 51. Measured phase passband response of Chebyshev filter.

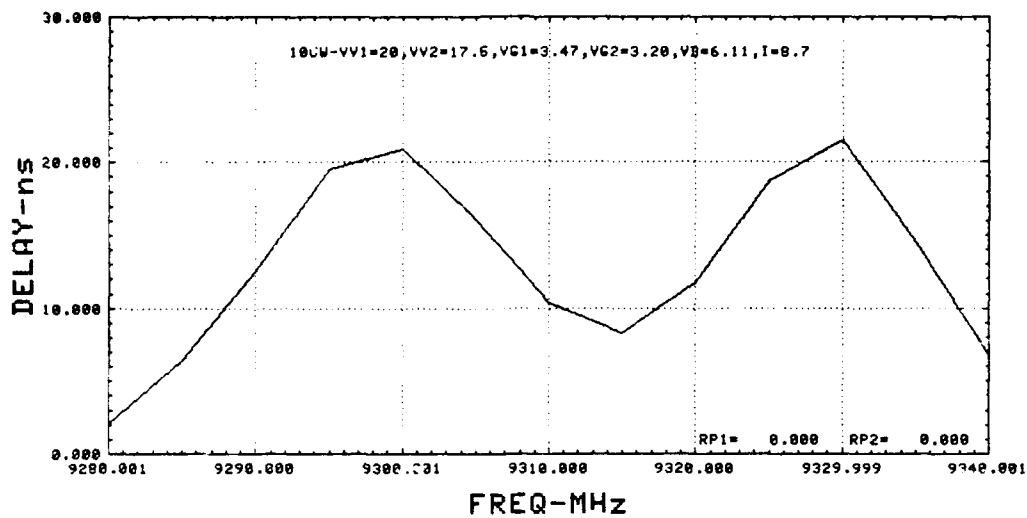


Figure 52. Measured group-delay passband response of Chebyshev filter.

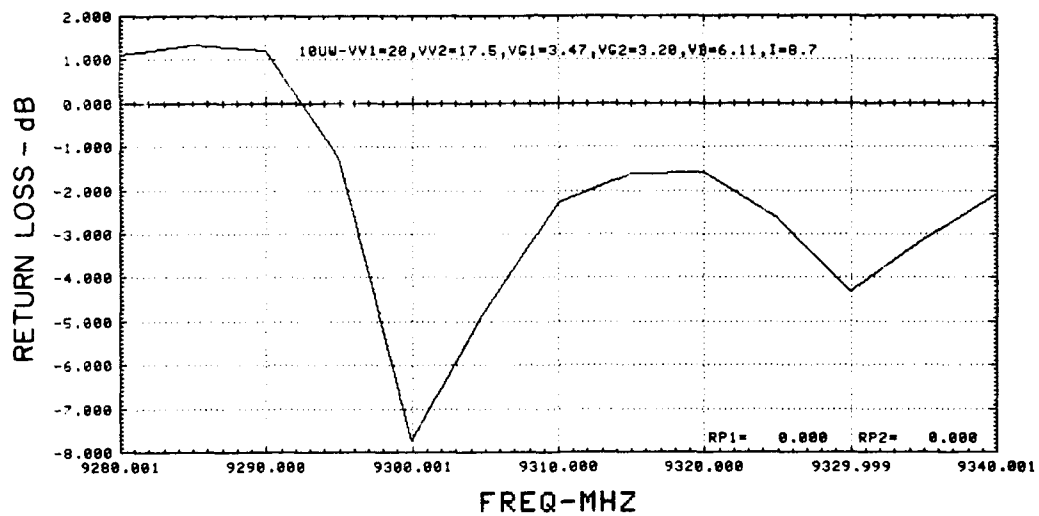


Figure 53. Measured passband return loss of Chebyshev filter.

### SECTION III

#### FINAL FILTER PERFORMANCE

##### A. SINGLE ELEMENT

The elements to be used in the construction of the two final two-section filters were constructed in modular form (see Fig. 15) as outlined in the previous sections. Each element was tested and adjusted individually in a test fixture, as shown in Fig. 16. The aim of the adjustments was to bring frequency, selectivity, and tuning voltages into a common range so that the largest range of operation can be attained when combining two elements into a two-section-filter arrangement. As indicated in the previous section, their range is determined by the frequency overlap of the two elements.

The plot of Fig. 54 shows the frequency vs varactor voltage characteristics of four elements that were prepared for the final filters. The frequencies correspond to gate-voltage adjustments for 0-dB transmission loss. These gate voltages for the four elements are plotted in Fig. 55. The particular 3-dB bandwidth that depends upon the input and output coupling is shown in Fig. 56. In the final use of these elements, no additional adjustments, other than voltage adjustments, were made on the element circuits.

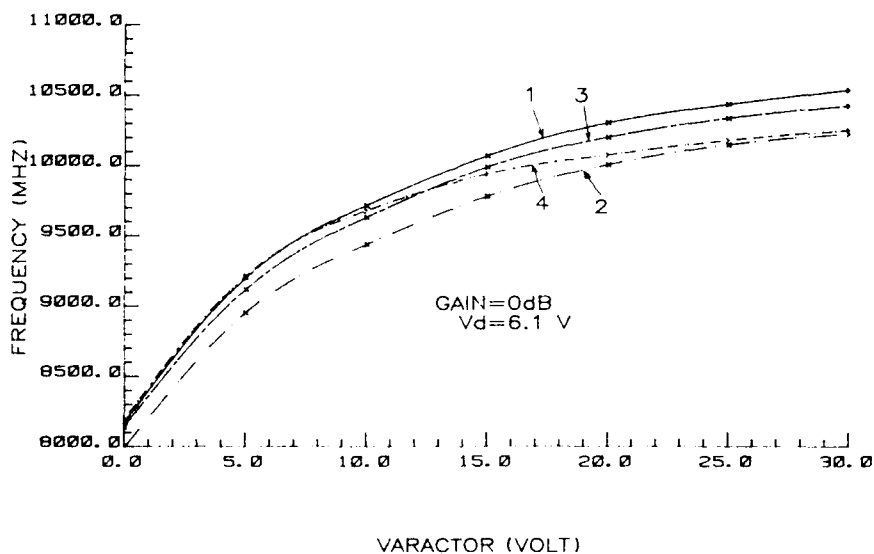


Figure 54. Measured midband frequency vs varactor voltage for four different resonant elements.

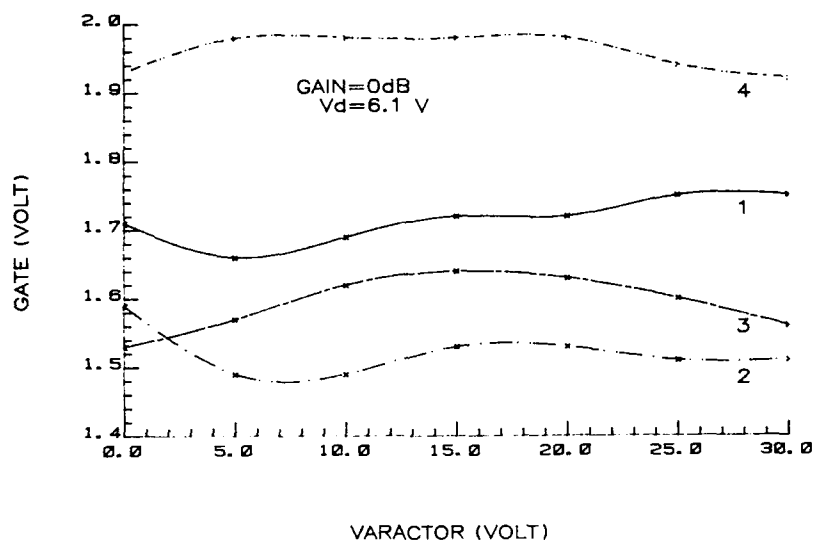


Figure 55. Measured gate voltage for 0-dB transmission loss of four different resonant elements at given varactor voltages.

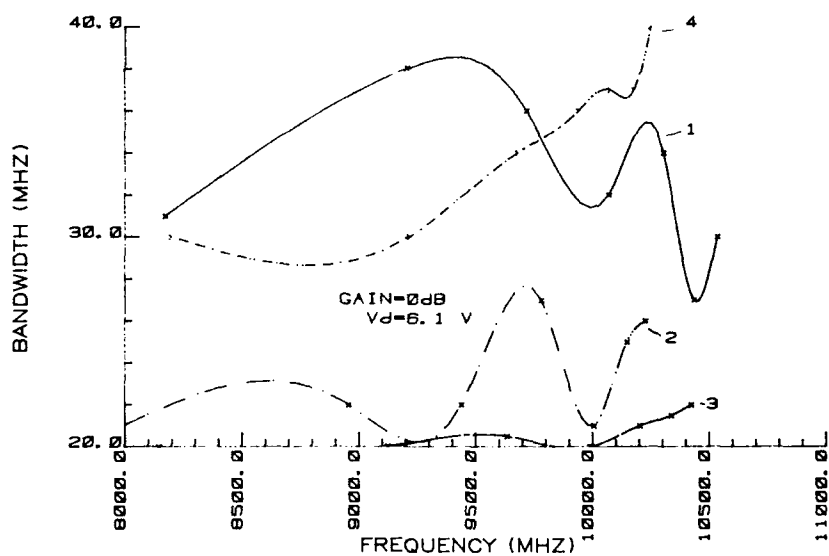


Figure 56. Measured 3-dB bandwidth of four different elements for given varactor voltage settings.

During the evaluation of the final filter elements it was noted that the tuning bandwidth ranged between 1.9 and 2.0 GHz, far short of the expected range of 2.4 to 2.6 GHz that was established in the prototype elements. The

reduced tuning range was traced to varactors received just before fabrication of the final elements. A check was made by exchanging the varactor of a prototype element with one of the newer ones. The 2.4-GHz tuning bandwidth decreased to 1.9 GHz, and selectivity for field coupling decreased as well. These measurements confirmed that the new varactors had higher resistive losses and smaller capacitance ratios when biased between the rated 0- to 30-V range. Since there was not sufficient time to order new varactors, the filter elements were completed with the varactors at hand.

## B. TWO-SECTION FILTER

The two-section filter consists of two modular elements that are capacitively coupled at input and output to short 50- $\Omega$  microstrip transmission lines that terminate in SMA connectors. Coupling between elements is also via capacitive proximity. Figure 57 is a photographic close-up of the assembled two-section-filter arrangement within a 38-mm x 35-mm x 20-mm brass enclosure. Capacitive feedthroughs provide access to the dc connections necessary for filter operation. A metallic partition between elements with an iris around the coupling tabs prevents both uncontrolled coupling between elements, and waveguide resonances of the enclosure that cause spurious rf-feedthrough. The photograph in Fig. 58 shows an overall view of a completely assembled filter with partitions in place but with cover removed.

Adjustments of the filter are first made with the cover and the partition removed. These adjustments entail capacitance changes obtainable from the coupling tabs that extend from each end of each resonant element, and appropriate voltage changes. The operating voltages of the two elements are adjusted to correspond approximately to those observed previously for each element at the same frequency within the tuning band. Keeping the two voltages of one element fixed, we made slight adjustments of the other voltage pair while observing the swept response of the filter on a network analyzer. Voltages are adjusted for best transmission response. The coupling to the transmission lines and the tabs between elements are adjusted next, until a true, well-matched, maximally flat response with desired 3-dB selectivity is obtained. Coupling adjustments are limited by stability considerations, and also have to be touched up subsequently to correct for effects caused by the

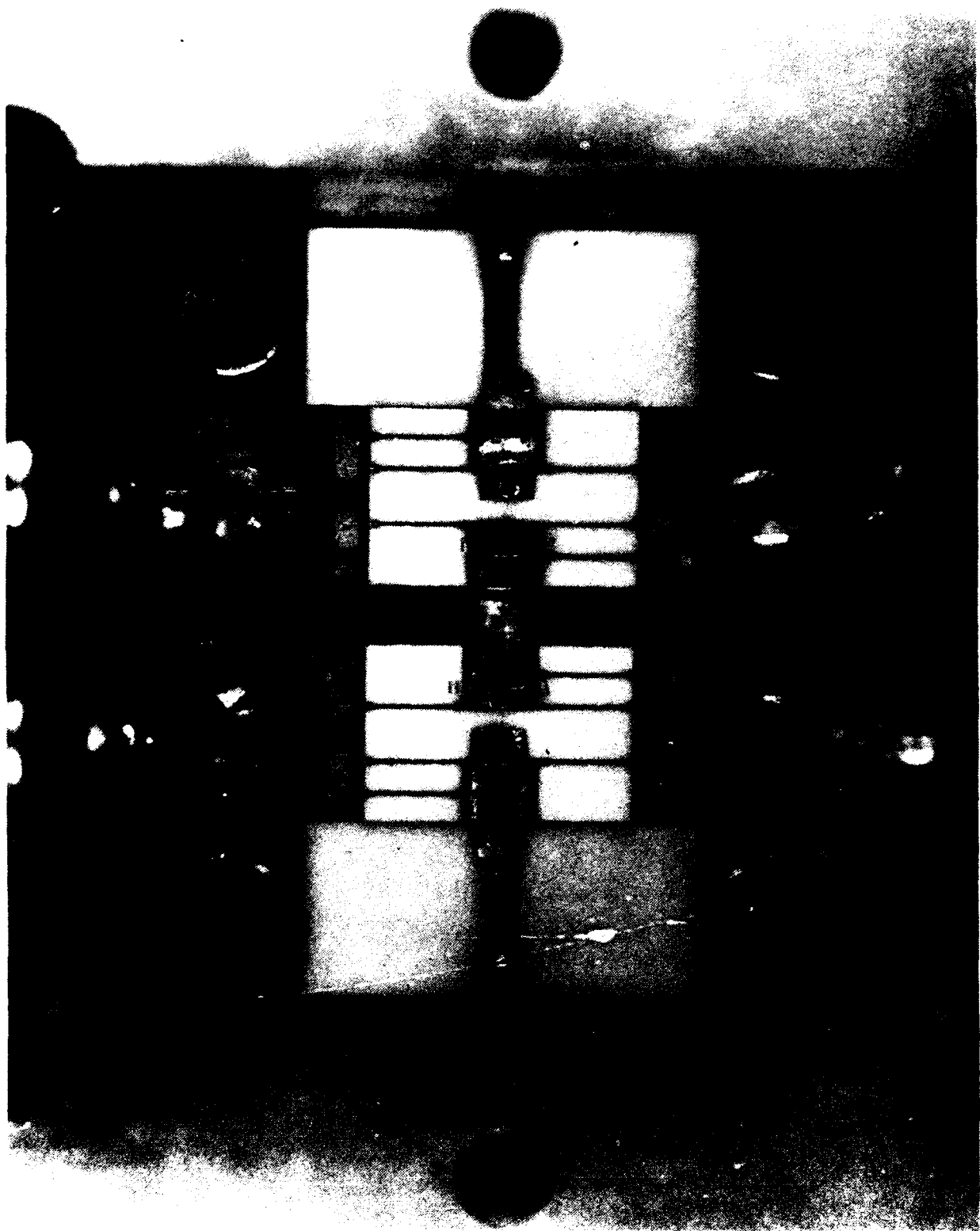


Figure 57. Photographic close-up of final two-section filter circuit.

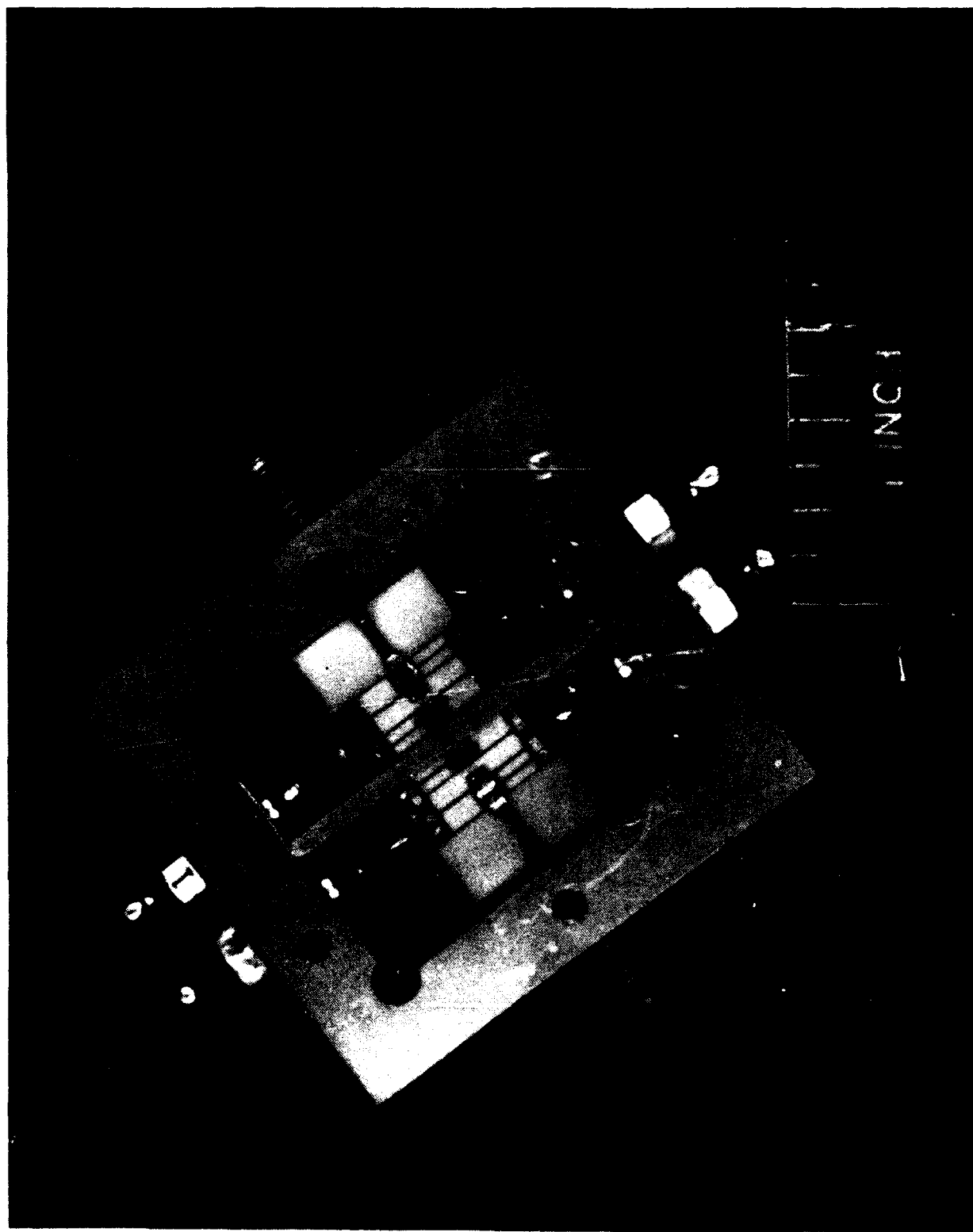


Figure 58. Photographic view of final two-section filter.

partitions and the cover. It was found that coupling adjustments first made at the upper-frequency end of the filter tuning band resulted in good filter operation over the entire band. This also avoids instabilities that tend to occur at the high-frequency end.

Two filters were fabricated, adjusted, and evaluated on both a test bench and an automatic network analyzer. In the following paragraphs the measured performance is described and some detailed results are shown. In the final evaluation, the case temperature of the filter was maintained at  $24.2 \pm 0.1^\circ\text{C}$  by means of a circulating-bath heatsink. The most important characteristics and effects of the filters were described previously in Sections II.D and II.E of this report.

Table 1 shows the voltages necessary for a given frequency when filter No. 1 was adjusted for a  $0 \pm 1\text{-dB}$  transmission loss. The same data in graphic form are shown in Fig. 59 for the varactor voltages vs frequency and in Fig. 60 for the gate voltages. The maximum tuning range of 2 GHz is determined by the mutually inclusive frequency range of the two elements in the 0- to 30-V tuning range of the varactors. As shown in Fig. 61, the corresponding 3-dB bandwidth over the tuning band varied between a low value of 18 MHz and a high value of 36 MHz. The bandwidth variations are mainly a function of varactor Q, a value that is about four times larger at the high frequency than at the low frequency. The coupling also varies as a function of frequency, but its effect upon bandwidth in this case is a compensating one. Also shown in Fig. 61 is the noise figure, which varies between 19.3 and 22.6 dB over the tuning frequency range. Figure 62 shows the measured gain and the VSWR as a function of frequency for the voltage setting corresponding to Figs. 59 and 60.

More detailed response results were obtained on the automatic network analyzer. The plot in Fig. 63 shows the transmission response at a particular set of voltages for both the forward and reverse directions of power flow. The plot in Fig. 64 shows the corresponding phase responses in the passband; Figs. 65 and 66 illustrate the reflection coefficients and group delays, respectively. The response symmetry is reasonably good. The effects of power input variations become apparent in the plot of Figs. 67 and 68, in which amplitude and group delays are shown for three different power input levels. A slight shift in midband frequency, a widening of the response, and a fall-off in relative transmitted power are noticeable.

TABLE 1. TWO-SECTION FILTER NO.1\*

Frequency (MHz)	$V_{V1}$ (V)	$V_{V2}$ (V)	$V_{G1}$ (V)	$V_{G2}$ (V)	BW (MHz)	Gain (dB)
8256	0.00	0.8	1.63	1.40	20	0.0
8580	1.10	2.5	1.62	1.34	18	1.0
8922	2.90	5.0	1.62	1.34	18	0.0
9412	6.67	10.0	1.62	1.34	20	0.0
9767	10.34	15.0	1.70	1.34	31	-1.0
9987	13.23	20.0	1.70	1.34	21	1.0
10147	15.72	25.0	1.70	1.34	30	1.0
10246	17.52	30.0	1.74	1.34	36	0.0

\* $P_{in} = -27$  dBm;  $V_D = 6.11$  V;  $T = 24.2 \pm 0.1^\circ\text{C}$ .

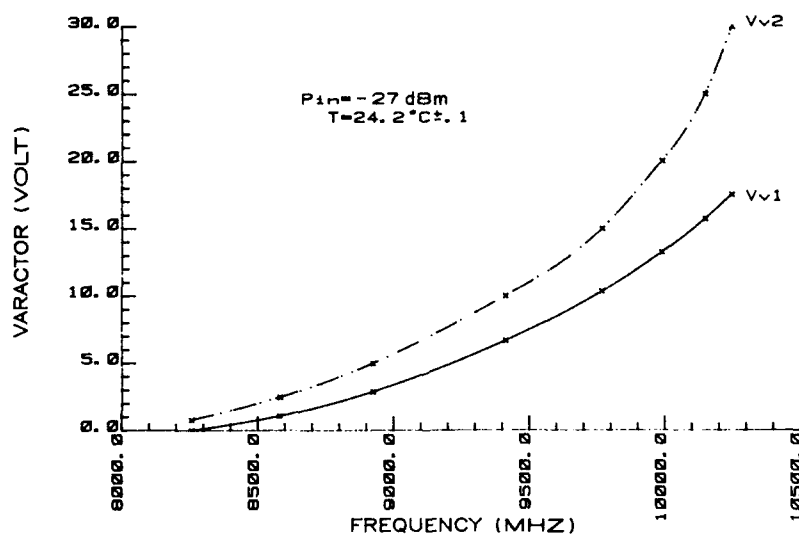


Figure 59. Measured varactor voltages vs midband frequency (final filter No. 1).

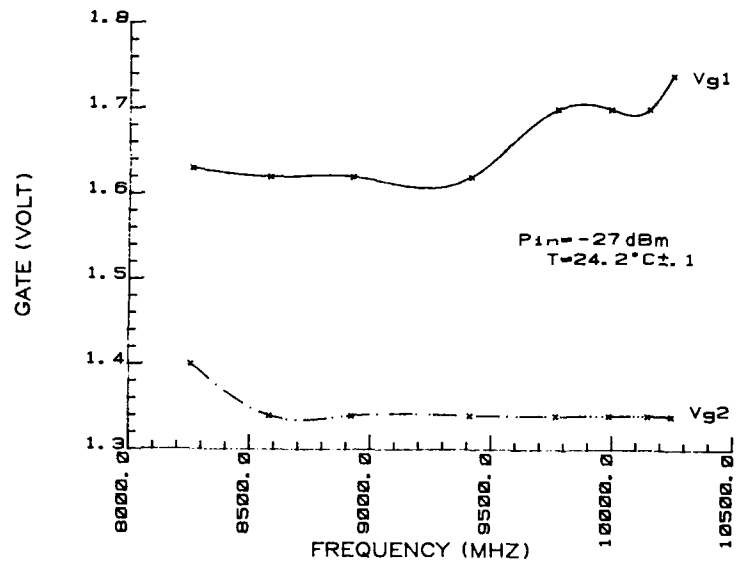


Figure 60. Measured gate voltages at midband frequency settings (final filter No. 1)

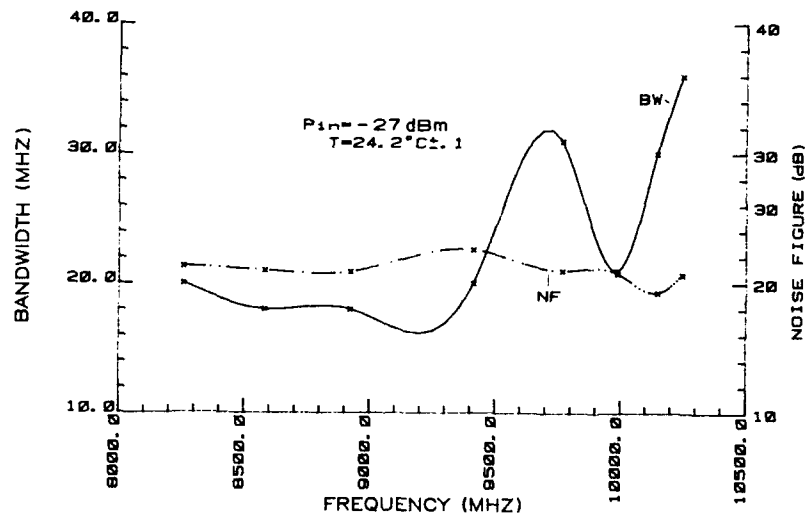


Figure 61. Measured 3-dB bandwidth and noise figure at midband frequency settings (final filter No. 1).

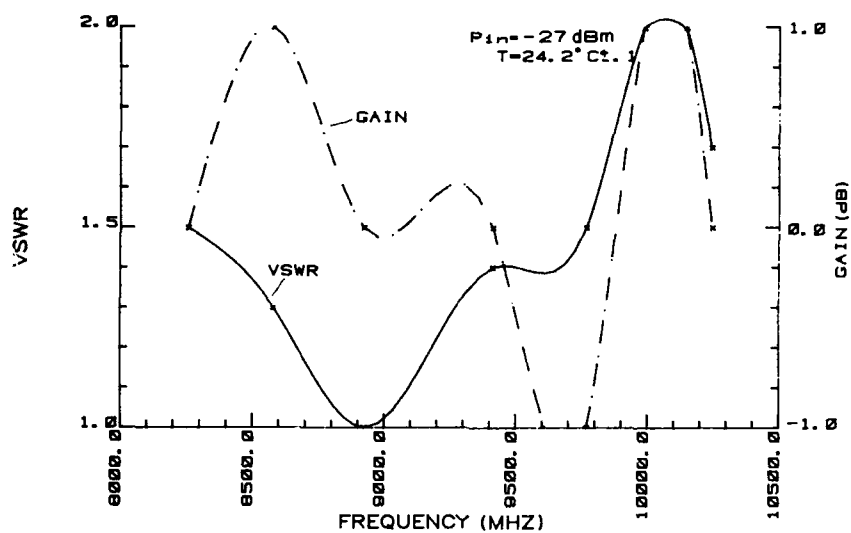


Figure 62. Measured transmission gain and VSWR at midband frequency settings (final filter No. 1).

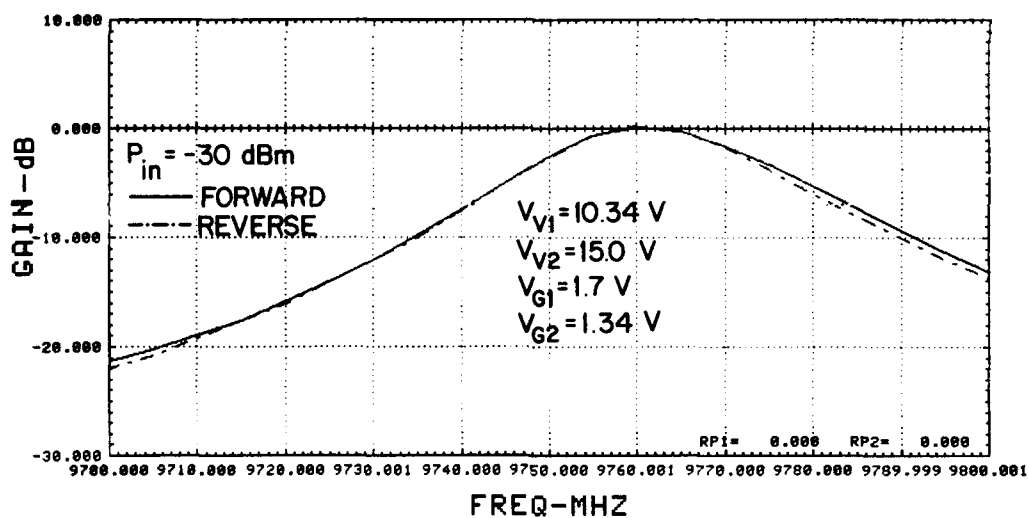


Figure 63. Measured transmission passband response for forward and reverse power flow (final filter No. 1).

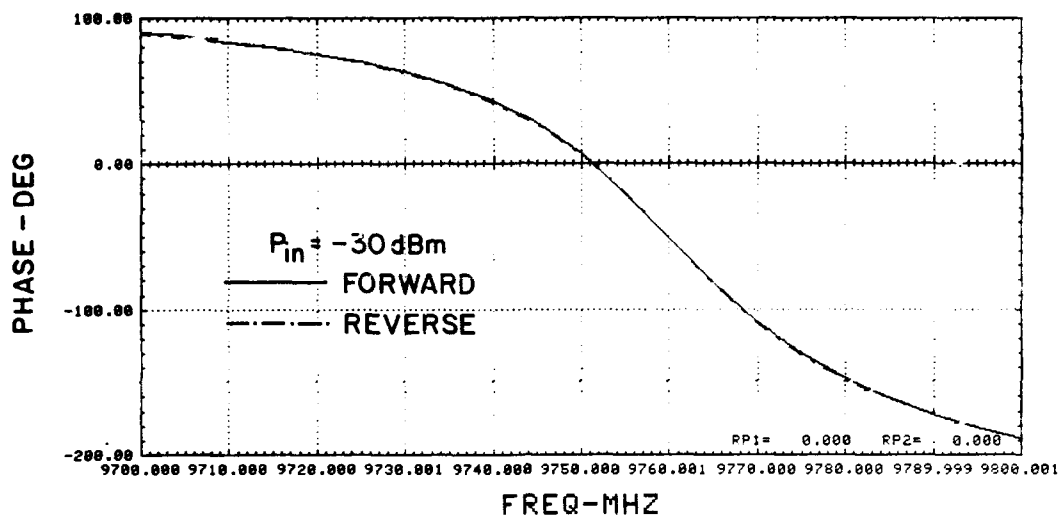


Figure 64. Measured phase passband response for forward and reverse power flow (final filter No. 1).

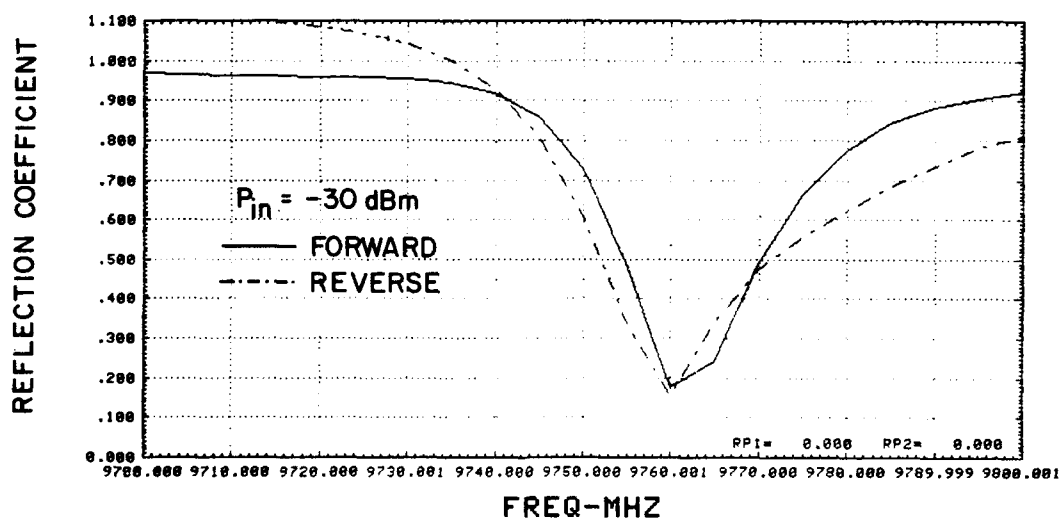


Figure 65. Measured input and output reflection coefficient in passband (final filter No. 1).

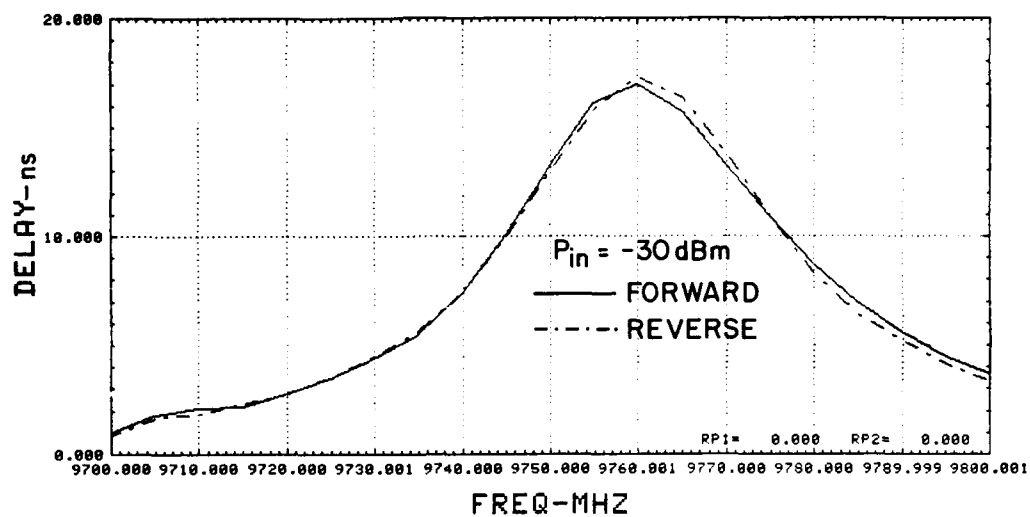


Figure 66. Measured forward and reverse group delay in passband (final filter No. 1).

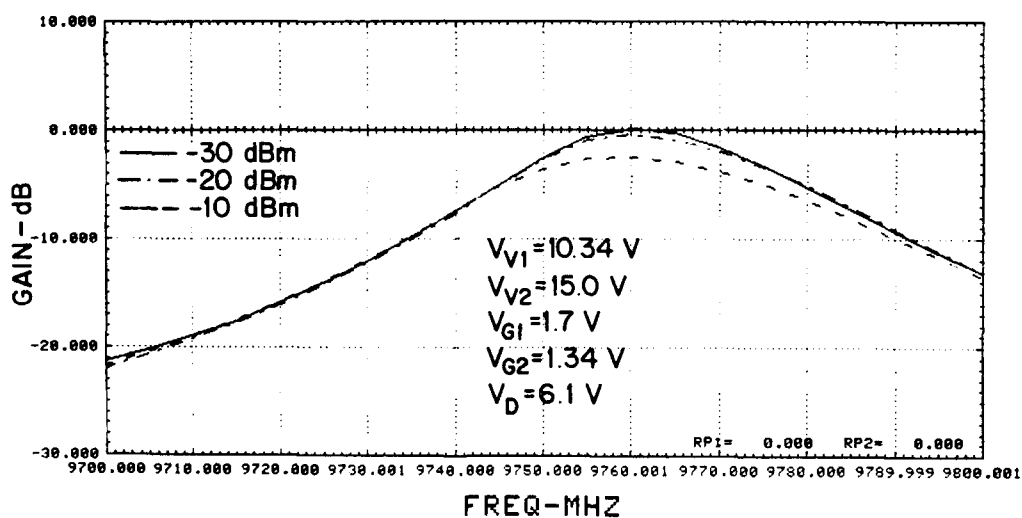


Figure 67. Measured midband response for three input power levels (final filter No. 1).

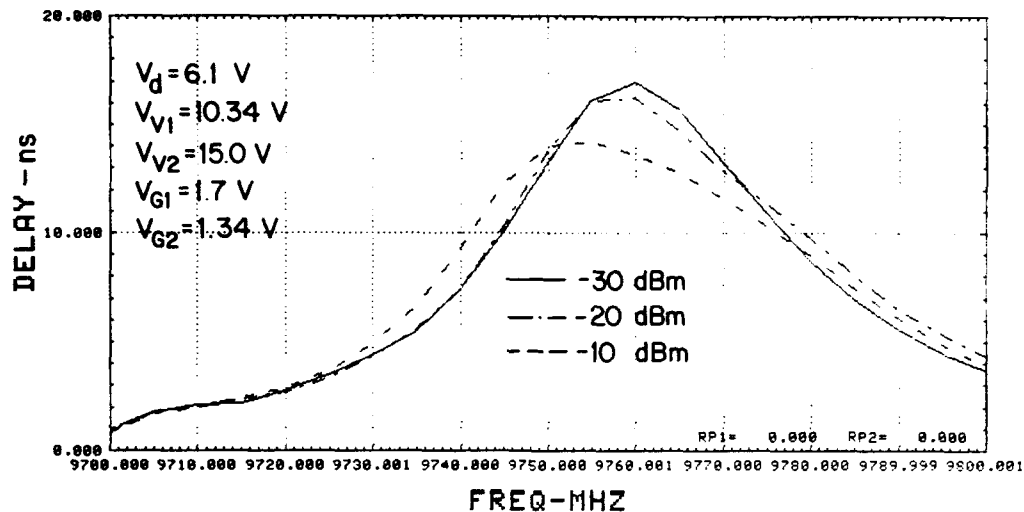


Figure 68. Measured group-delay midband response for three input power levels (final filter No. 1).

Table 2 shows the voltages necessary at any given frequency for filter No. 2. The filter was adjusted for  $0 \pm 2$ -dB transmission loss. Figures 69 and 70 show the required varactor and gate voltages; the corresponding gain and VSWR are shown in Fig. 71; the 3-dB bandwidth and noise figure are shown in Fig. 72. These measured characteristics were similar to the ones observed in filter No. 1.

TABLE 2. TWO-SECTION FILTER NO. 2\*

Frequency (MHz)	$V_{V1}$ (V)	$V_{V2}$ (V)	$V_{G1}$ (V)	$V_{G2}$ (V)	BW (MHz)	Gain (dB)
8274	0.26	0.0	1.71	2.04	36	-4.0
8842	2.95	2.5	1.69	1.96	35	-1.0
9185	5.48	5.0	1.73	1.94	32	0.0
9661	10.36	10.0	1.76	1.94	34	0.0
9941	14.33	15.0	1.82	1.94	36	-0.5
10118	17.70	20.0	1.82	1.94	36	-1.0
10224	20.60	25.0	1.82	1.94	36	-1.0
10297	23.20	30.0	1.81	1.94	39	-1.5

\* $P_{in} = -27$  dBm;  $V_D = 6.11$  V;  $T = 24.2 \pm 0.1^\circ\text{C}$ .

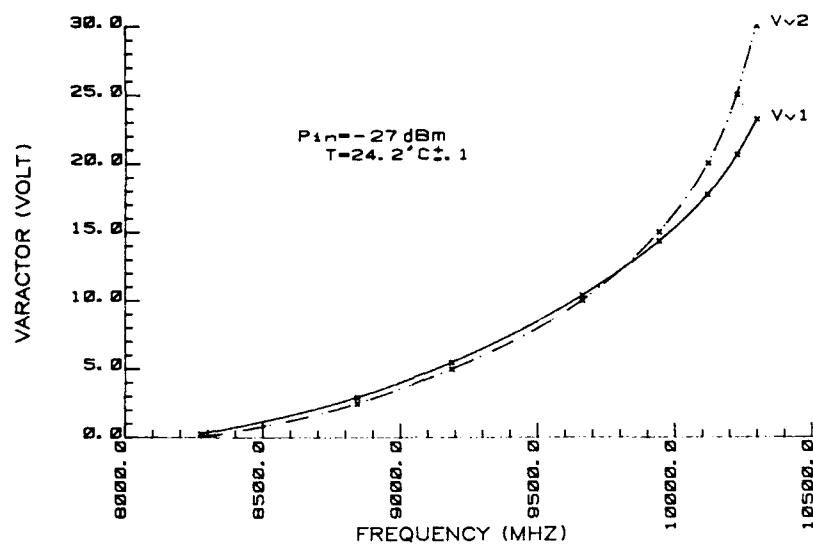


Figure 69. Measured varactor voltage for each element at given midband frequencies (final filter No. 2).

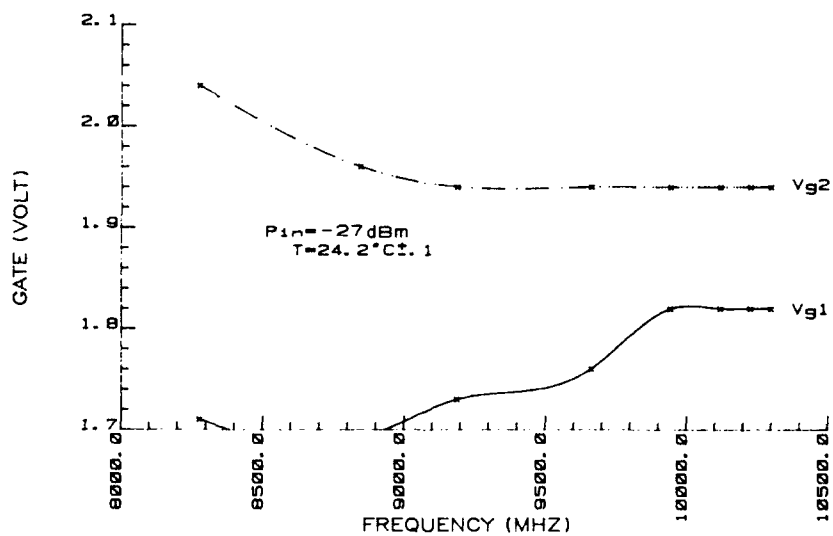


Figure 70. Measured gate voltages for each element at given midband frequencies (final filter No. 2).

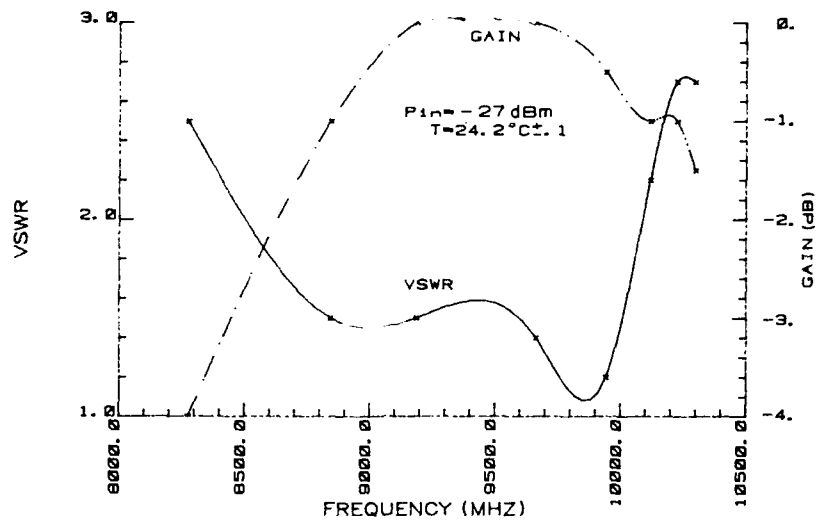


Figure 71. Measured transmission gain and VSWR vs midband frequency (final filter No. 2).

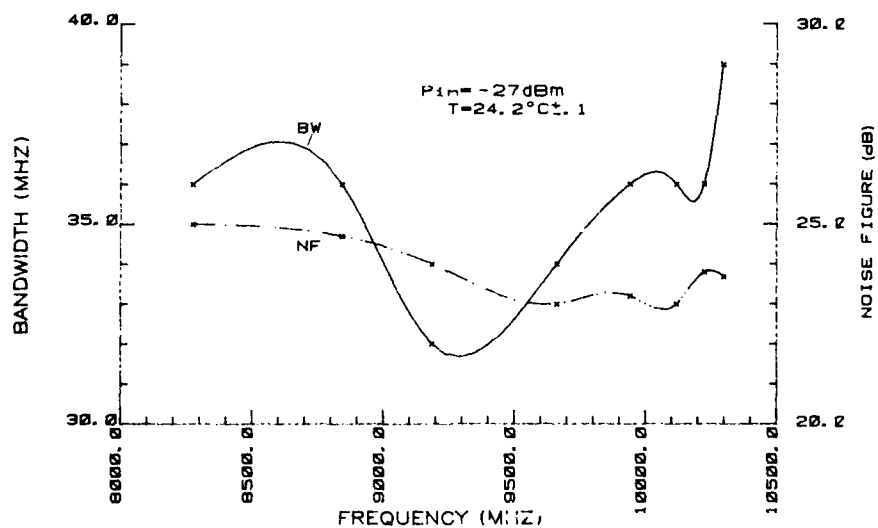


Figure 72. Measured 3-dB bandwidth and noise figure vs midband frequency (final filter No. 2).

The sequence of plots in Figs. 73 to 76 demonstrates symmetric performance of the filter with respect to direction of power flow. Figures 77 and 78 show the effect of power input on transmission and delay responses. Symmetry and power input sensitivity were similar to the values observed in filter No. 1.

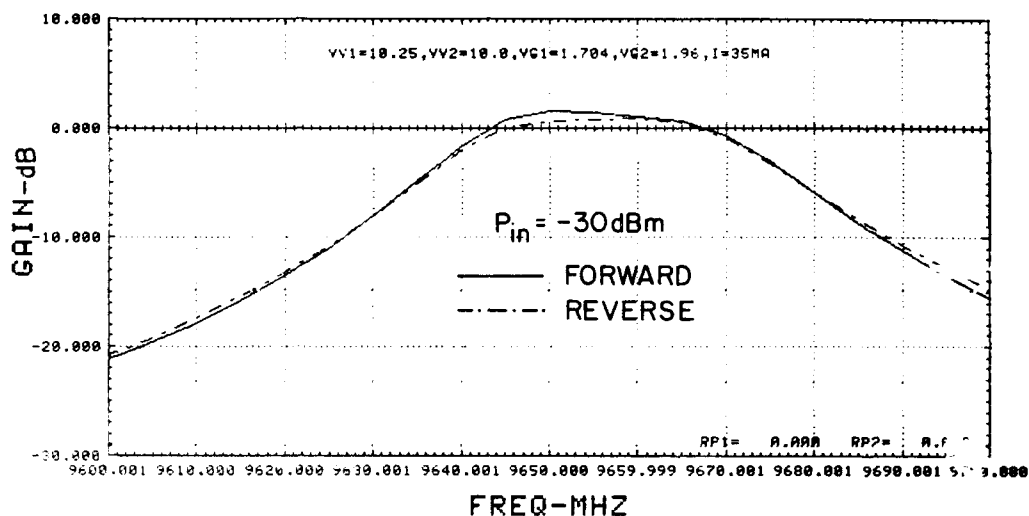


Figure 73. Measured transmission passband response for forward and reverse power flow (final filter No. 2).

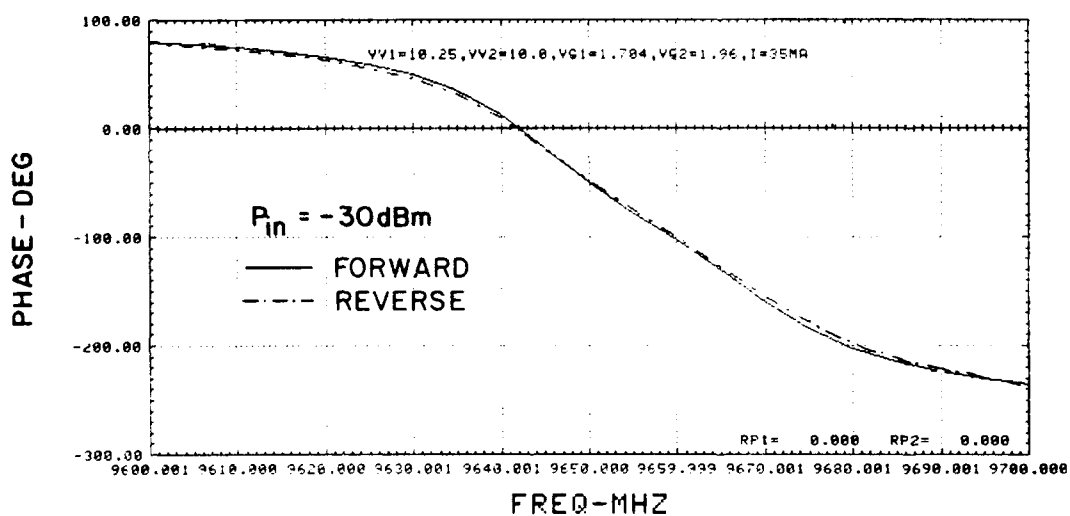


Figure 74. Measured phase passband response, forward and reverse (final filter No. 2).

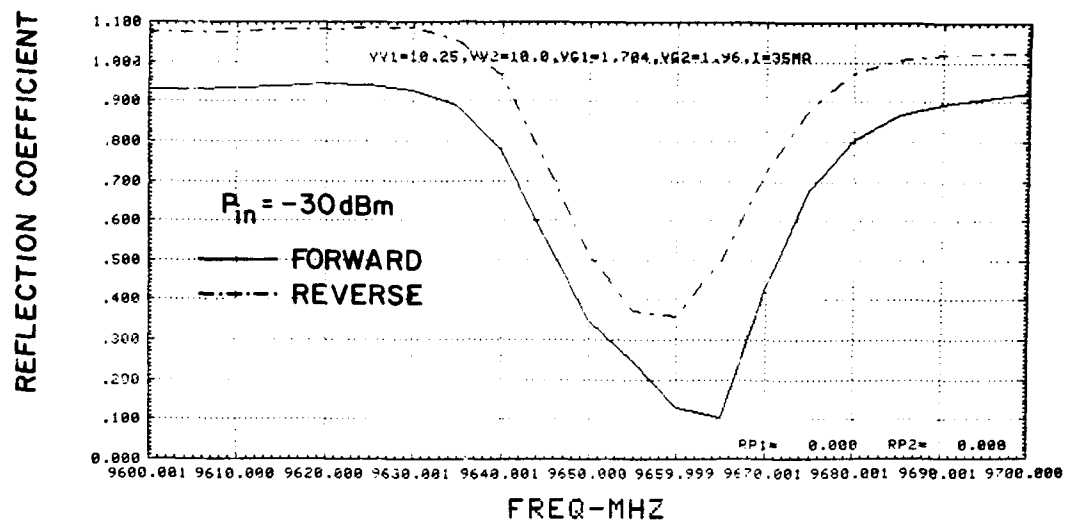


Figure 75. Measured input and output reflection coefficient frequency response (final filter No. 2).

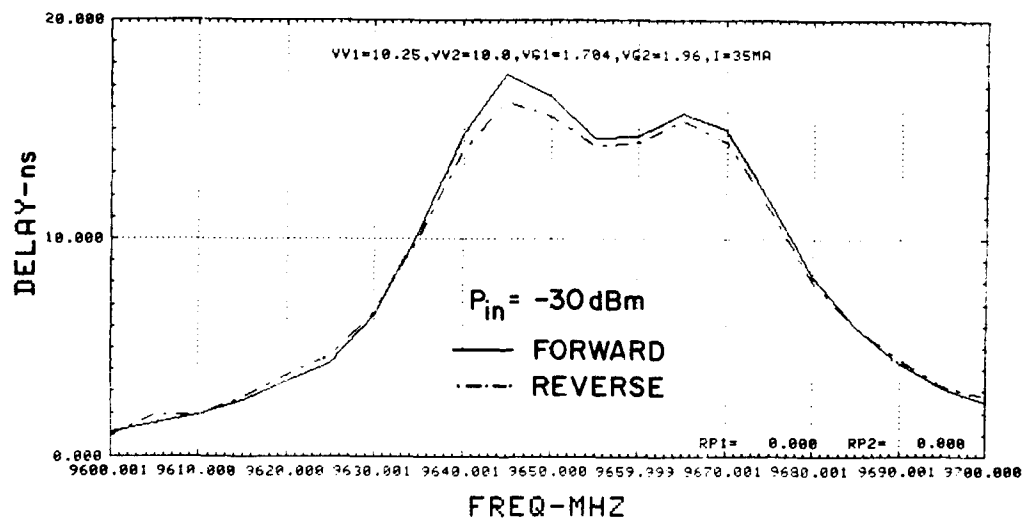


Figure 76. Measured forward and reverse group-delay passband response (final filter No. 2).

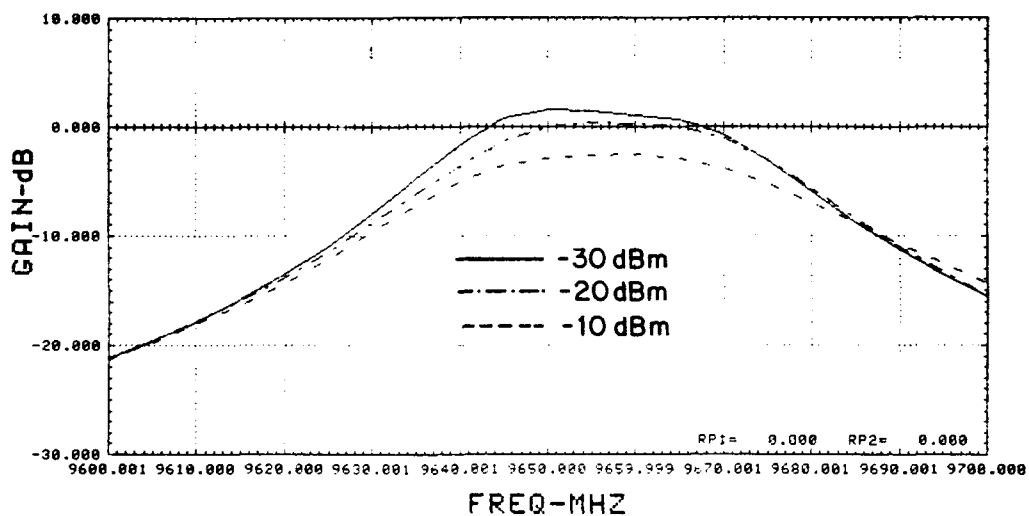


Figure 77. Measured midband response for three input power levels (final filter No. 2).

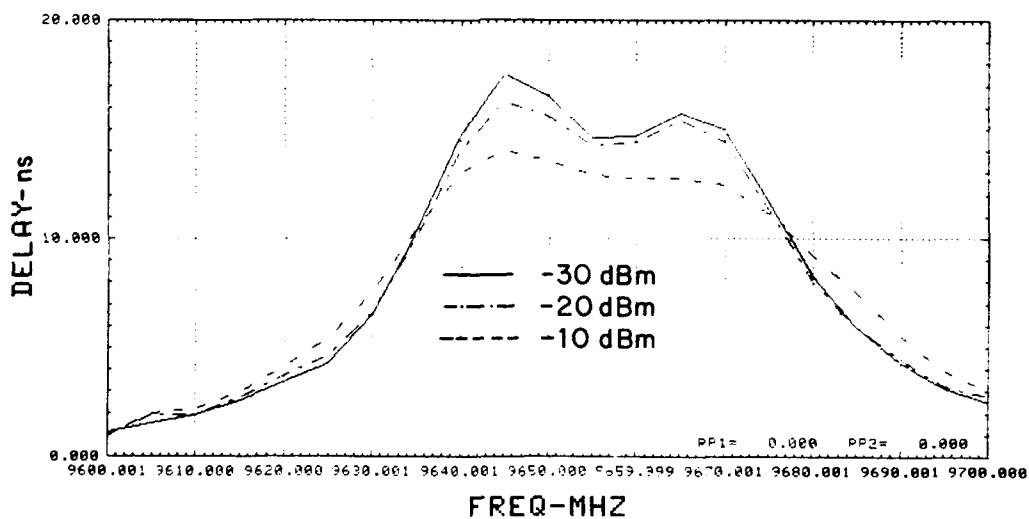


Figure 78. Measured group-delay midband response for three input power levels (final filter No. 2).

The relatively similar performance of the two filters was attained without special prescreening of parts and without elaborate matching techniques. Thus, the reproducibility is good, and better uniformity and better overall filter performance can be expected with improved fabrication controls. Resetability of obtained results is a function of case temperature, device dissipation, and instrument accuracy.

## SECTION IV

### CONCLUSIONS AND RECOMMENDATIONS

The Phase II, Task 2 program achievements, findings, and recommendations can be summarized as follows:

- The tunable resonant element developed during Task 1 was redesigned to eliminate a variety of detrimental effects. This new element uses only one FET and one varactor while maintaining good electrical symmetry.
- Filter performance is essentially symmetric with respect to power flow. Symmetry suffers with "near instability" adjustments.
- Element stability was improved by eliminating critical rf-choke lines.
- Tuning bandwidth capabilities of 3.6 GHz were demonstrated on a single resonant element.
- Two two-section filters that are tunable over a frequency band of 2.0 GHz  $\pm$ 20 MHz in the 8.2- to 10.3-GHz frequency range were completed and tested.
- A 29  $\pm$ 11-MHz 3-dB bandwidth was demonstrated over the entire tuning range.
- Response adjustments from maximally flat to Chebyshev with 2-dB ripple could be achieved with proper coupling control.
- Stability considerations limit the response bandwidth of multisection filters to about 20 MHz.
- Power input level sensitivity of responses increases with increasing selectivity. For a 3-dB bandwidth of 30 MHz, a power input level of -10 dBm causes only minor response degradations. We recommend study of this problem aiming at a level increase of 20 dB.
- Noise figure is a function of FET feedback arrangement and is about 18 dB for a single element. There seems to be no straightforward cascading relationship for multiple-element filters. We recommend further work to improve the noise figure and to investigate multiple-element noise relationships.
- Future tasks should concentrate on improvements with respect to power input level, noise figure, and addressing and driving circuits that determine frequency setting and ultimate tuning speed.

## REFERENCES

1. A. Presser, "Ultra-Fast Tunable Microwave Filter," Final Report, Contract No. N00173-77-C-0201, Aug. 1978.
2. A. Presser, "Ultra-Fast Tunable Microwave Filter," Final Report, Phase II, Task 1, Contract No. N00173-79-C-0186, Aug. 1980.
3. G. L. Matthaei et al., Microwave Filters, Impedance-Matching Networks and Coupling Structures (McGraw-Hill Book Co., New York 1964), p. 421.
4. J. F. Cline et al., "Tunable Passive Multi-Couplers Employing Minimum Loss Filters," IRE Trans. PGMTT-7, 121 (Jan. 1959).
5. S. B. Cohn, "Dissipation Loss in Multiple-Coupled Resonator Filters," Proc. IRE 47, 1342 (Aug. 1959).
6. P. Penfield, Jr., and R. P. Rafuse, Varactor Applications (MIT Press, Cambridge, MA, 1962).
7. P. Wolf, "Microwave Properties of Schottky-Barrier Field-Effect Transistors," IBM J. Res. Dev. 14, 125 (March 1970).